© 2018. Published by The Company of Biologists Ltd | Journal of Cell Science (2018) 131, jcs214726. doi:10.1242/jcs.214726

RESEARCH ARTICLE

Cyclin D1 depletion interferes with oxidative balance and promotes cancer cell senescence

Phatthamon Laphanuwat[1], Pornlada Likasitwatanakul[1], Gunya Sittithumcharee[1], Araya Thaphaengphan[1], Nussara Chomanee[2], Orawan Suppramote[1], Nuttavadee Ketaroonrut[1], Komgrid Charngkaew[2], Eric W.-F. Lam[3], Seiji Okada[4], Uraiwan Panich[1], Somponnat Sampattavanich[1] and Siwanon Jirawatnotai[1,*]

ABSTRACT

Expression of cyclin D1 (*CCND1*) is required for cancer cell survival and proliferation. This is presumably due to the role of cyclin D1 in inactivation of the RB tumor suppressor. Here, we investigated the pro-survival function of cyclin D1 in a number of cancer cell lines. We found that cyclin D1 depletion facilitated cellular senescence in several cancer cell lines. Senescence triggered by cyclin D1 depletion was more extensive than that caused by the prolonged CDK4 inhibition. Intriguingly, the senescence caused by cyclin D1 depletion was independent of RB status of the cancer cell. We identified a build-up of intracellular reactive oxygen species in the cancer cells that underwent senescence upon depletion of cyclin D1 but not in those cells where CDK4 was inhibited. The higher ROS levels were responsible for the cell senescence, which was instigated by the p38-JNK-FOXO3a-p27 pathway. Therefore, expression of cyclin D1 prevents cancer cells from undergoing senescence, at least partially, by keeping the level of intracellular oxidative stress at a tolerable sub-lethal level. Depletion of cyclin D1 promotes the RB-independent pro-senescence pathway and the cancer cells then succumb to the endogenous oxidative stress levels.

This article has an associated First Person interview with the first author of the paper.

KEY WORDS: CDK4, Cyclin D1, FOXO3a, Retinoblastoma protein, Oxidative stress, Senescence

INTRODUCTION

Cyclin D1 is a cell cycle regulatory protein, which is amplified and overexpressed in a large number of human cancers (Sukov et al., 2009; Musgrove et al., 2011; Lee et al., 2016). Expression of cyclin D1 is essential for oncogenic transformation as well as for cancer cell survival. Activation of the Kras or HER2 pathways targeted in mouse breast tissue resulted in breast cancer, but failed to induce any tumors in breasts of cyclin D1-deficient mice (Yu et al., 2001). In addition, shutdown of cyclin D1 expression in breast tumors resulted in cessation of tumor growth associated with cancer cell senescence (Choi et al., 2012).

The cancer-supporting role of cyclin D1 in cancer formation and survival represents a curious circumstance, in that although it is required for cancer formation, cyclin D1 does not appear to be a strong cancer driver. Forced expression of cyclin D1 in mouse models did not promote cancer formation until after a very long latency (Wang et al., 1994; Casimiro and Pestell, 2012). Thus, expression of cyclin D1 may be required to support oncogenic transformation, possibly by creating permissive cellular conditions for cancer cell transformation.

The best-described function of cyclin D1 is in the formation of complexes and activation of cyclin-dependent kinase 4 or 6 (CDK4/6). The cyclin-D1–CDK4/6 complex phosphorylates and inactivates retinoblastoma (RB) protein which allows the cell to enter S phase from G1. Emerging evidence suggests that cyclin D1 also holds several cancer-related roles beyond the canonical RB inactivation. These proposed additional roles include functions in transcriptional control, homologous-mediated DNA repair, differentiation, migration and mitochondria regulation etc. (Hydbring et al., 2016). It remains unclear whether any of these non-canonical roles has a role in cancer formation.

Cellular redox status has been shown to influence several biological processes (Trachootham et al., 2009). Oxidative equilibrium relies on a well-regulated rate of production versus elimination of oxidative species in the cell. Oxidative imbalance has been demonstrated to influence cellular behavior, and to underline several pathological conditions, including cancer (Vurusaner et al., 2012). Here, we investigated the anti-senescence role of cyclin D1 in cancer cells. We showed that cyclin D1 expression is essential for cancer cells to remain in the proliferative and non-senescence stage, by maintaining oxidative stress in cancer cells at a low sub-lethal level, and stops the cells succumbing to oxidative stress-induced senescence.

RESULTS

Cyclin D1 depletion results in cancer senescence in several types of human cancer

Expression of cyclin D1 was shown to be indispensable for preventing cell senescence in cancer cells *in vivo* and *in vitro* (Choi et al., 2012; Brown et al., 2012). However, it is not known whether the anti-senescence role of cyclin D1 is universal in every cellular context, as in a number cell types and certain circumstances, cell division may take place without cyclin D1 (Sherr and Roberts, 2004). Thus, we examined the role of cyclin D1 in cancer cell senescence by using cyclin D1-specific RNA interference to deplete cyclin D1 in the following human cancer cell lines: MDA-MB-175, ZR-75-1, MDA-MB-134, T47D, SKBR3 and MCF7 (breast cancer); KKU-156, KKU-214 and TYBDC-1 (cholangiocarcinoma); and

[1]Siriraj Center of Research for Excellence (SiCORE) for Systems Pharmacology, Department of Pharmacology, Faculty of Medicine, Siriraj Hospital, Mahidol University, Bangkok 10700, Thailand. [2]Department of Pathology, Faculty of Medicine, Siriraj Hospital, Mahidol University, Bangkok 10700, Thailand. [3]Department of Surgery and Cancer, Imperial College London, Hammersmith Hospital Campus, London W12 0NN, UK. [4]Division of Hematopoiesis, Center for AIDS Research, Kumamoto University, 2-2-1 Honjo Chuo-ku, Kumamoto 860-0811, Japan.

*Author for correspondence (siwanon.jir@mahidol.ac.th)

G.S., 0000-0001-5855-5285; S.J., 0000-0002-8252-3782

Received 5 January 2018; Accepted 22 May 2018

Journal of Cell Science (2018) 131, jcs214726. doi:10.1242/jcs.214726

UMSCC2 (squamous cell carcinoma). After 4 days of cyclin D1 depletion, 6 of 10 cell lines demonstrated clear signs of cellular senescence, gauged by a marked increase in the number of cells with expression of an established senescence marker, senescence-associated β-galactosidase (SA-β-Gal) (Fig. 1A and Fig. S1A). The senescent cells were from three tissues of origin. We noticed that these cell

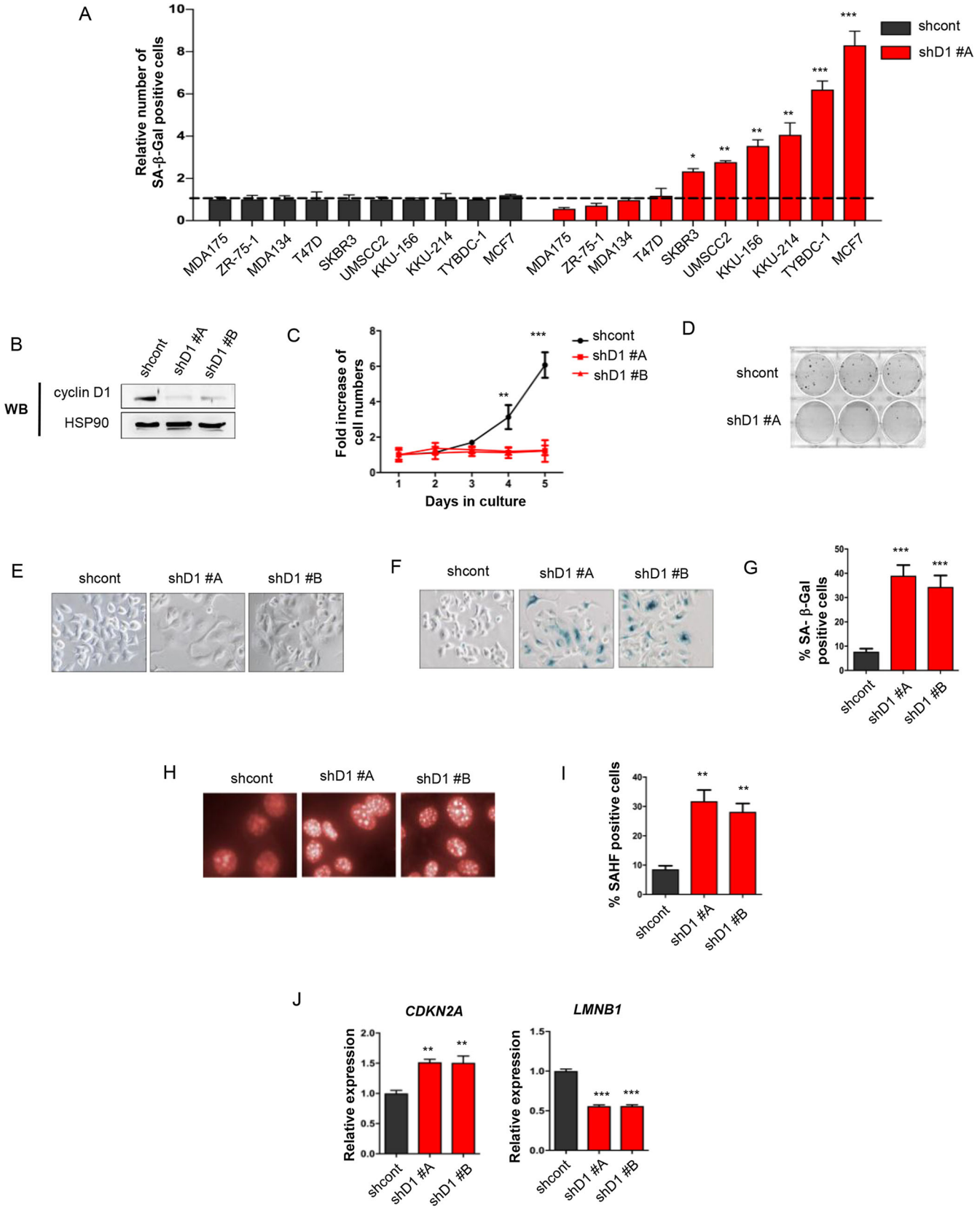

Fig. 1. See next page for legend.

Journal of Cell Science (2018) 131, jcs214726. doi:10.1242/jcs.214726

Fig. 1. Depletion of cyclin D1 causes cellular senescence in cancer cell lines. (A) Cancer cell lines were transduced with lentivirus expressing non-targeting shRNA (shcont) or shRNA against cyclin D1 (shD1#A) and SA-β-Gal-positive cells were counted on day 4 after transduction. Bars show mean±s.d. number of SA-β-Gal-positive cells (n=500). (B) Western blot (WB) analysis of cyclin D1 expression after treatment with two independent shRNAs (shD1#A and shD1#B). Heat shock protein 90 (HSP90) was used as a loading control. (C) Growth curves of cyclin D1-depleted MCF7 cells (shD1#A and shD1#B). (D) Colony-forming assay of cyclin D1-depleted MCF7 cells. (E) Cellular morphology and (F) SA-β-Gal expression of cyclin D1-depleted MCF7 cells at day 4 after cyclin D1 depletion. Positive cells appear in greenish-blue. (G) Percentage of SA-β-Gal-positive cells from F. Bars represent mean±s.d. number of SA-β-Gal-positive cells. (H) Immunofluorescence staining (IF) of SAHF in cyclin D1-depleted cells. The results showed trimethyl-histoneH3 at Lys9 (H3K9) foci (bright foci) in cyclin D1-depleted MCF7 cells. Cells with more than five foci per nucleus are considered positive. (I) Percentage of SAHF-positive cells from H. (J) Upregulation of *CDKN2A* (p16) and downregulation of *LMNB1* (lamin B) in cyclin D1-depleted cells, as measured by qRT-PCR. Bars represent the means±s.d. of three independent experiments. Statistical significance was determined with Student's t-test (*P≤0.05, **P≤0.01 and ***P≤0.001).

lines expressed varying levels of endogenous cyclin D1 (Fig. S1B). Therefore, the anti-senescence function of cyclin D1 was not ubiquitous among all of the cancer cell lines, and this role was not correlated with the pre-existing level of expression of cyclin D1 in each cancer cell line.

We carefully verified the senescence induced by cyclin D1 depletion by examining the characteristics of these cells. Depletion of cyclin D1 by two independent cyclin D1-specific short-hairpin RNAs (shRNAs) produced the same outcomes: they inhibited cancer cell division. Cyclin D1-depleted cells remained non-proliferative after 5 days in culture (Fig. 1B,C), and did not re-enter the cell cycle after long-term culture (Fig. 1D). Cyclin D1-depleted cells appeared flattened with large volumes of cytoplasm (Fig. 1E) and were positive for SA-β-Gal staining (Fig. 1F,G). Cyclin D1-depleted cells also showed a significant increase in senescence-associated heterochromatin foci (SAHF), another putative marker for cellular senescence (Narita et al., 2003) (Fig. 1H,I). Lastly, expression of *CDKN2A* mRNA was upregulated (Rayess et al., 2012) and *LMNB1* mRNA was downregulated (Freund et al., 2012) (Fig. 1J), confirming that these cells underwent cellular senescence after cyclin D1 depletion. These results indicate that cyclin D1 depletion enables cancer cells to undergo authentic cellular senescence. In addition, we found that re-expression of cyclin D1 neither restored cell proliferation nor reduced SAHF in the cyclin D1-depleted cells (Fig. S1C-E), indicating that, once triggered, the senescence was irreversible. To understand the nature of the senescence observed in cyclin D1-depleted cells, we studied the timing of senescence initiation. We found that a significant number of SAHF-positive cells were detected 48 h after transfection of cyclin D1-specific small interfering RNA (siD1), which correlated with the depletion of cyclin D1 protein (Fig. 2A,B). We also observed a moderate increase of cancer cell apoptosis upon cyclin D1 depletion. The increased apoptosis was not observed in control cells, or in cancer cells treated with PD0332991, a specific CDK4/6 inhibitor (Fig. S2A). Apoptosis associated with cyclin D1 depletion might be a result of DNA damage, since cyclin D1 depletion-induced senescent cells contained increased levels of the DNA damage marker γH2AX, which were comparable to levels obtained with 50-100 μM H_2O_2 (Fig. S2B).

A previous study demonstrated that prolonged inhibition of CDK4 activity by CDK4/6 inhibitor also resulted in cancer cell senescence (Otto and Sicinski, 2017). We treated MCF7 cells with PD0332991 and observed that CDK4/6 inhibition resulted in growth arrest and senescence (Fig. S3A,B, respectively). However, prolonged inhibition caused a delayed type of senescence that became significant only at 96 h after the 0.5 μM PD0332991 treatment. In agreement with that, suppression of CDK4 activity by CDK4-specific siRNA also resulted in the delayed type of senescence (Fig. S3C,D). These results suggested that depletion of cyclin D1 may be more robust than inhibition of CDK4/6 kinase activity as a trigger for cancer cell senescence. Finally, we showed that expression of the kinase-dead version of cyclin D1 (K112E) significantly reduced

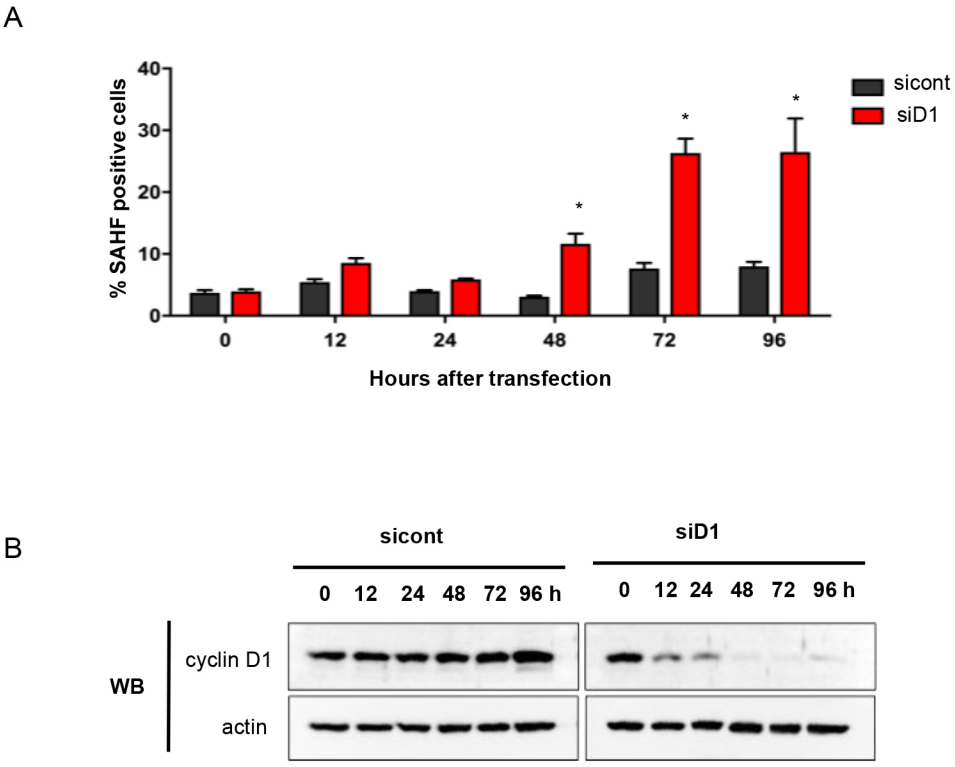

Fig. 2. Association between cyclin D1 downregulation and senescence. (A) Cellular senescence in cyclin D1-depleted cancer cells at various time points. MCF7 cells were transfected with either control non-targeting siRNA (sicont) or cyclin D1-specific siRNA (siD1) and SAHF-positive cell numbers were determined at indicated time points. Bars represent percentage of SAHF-positive cells. (B) Expression of cyclin D1 after siRNA-mediated depletion. MCF7 cells were transfected with either sicont or siD1. Protein lysates were harvested at indicated time points after siRNA transfection. Western blot (WB) analysis shows cyclin D1 depletion efficiency. Actin was used as a loading control. Statistical significance was determined with Student's t-test (*P≤0.05).

Journal of Cell Science (2018) 131, jcs214726. doi:10.1242/jcs.214726

senescence in cyclin D1-depleted cells under cyclin D1 depletion conditions (Fig. S3E,F); therefore, CDK4 activity is not involved in the early-onset senescence observed in cyclin D1-depleted cells.

The anti-senescence role of cyclin D1 is independent of its RB-inactivation function

In order to investigate whether the senescence observed in cyclin D1-depleted cancer cells was mediated by RB, we established a RB-deficient MCF7 cell line by stably expressing RB-specific shRNA (Fig. 3A). We verified that these RB-deficient cells were unaffected by inhibition of CDK4 kinase activity by treating the cells with PD0332991. MCF7-shRB cells continued to proliferate under treatment, indicating that without RB, cyclin D1-CDK4 kinase was no longer required for these cells to proliferate (Fig. 3B). Consistent with this, MCF7-shRB cells did not undergo senescence under prolonged 0.5 µM PD0332991 treatment (Fig. 3C and Fig. S3G).

Interestingly, we found that cyclin D1 depletion effectively inhibited MCF7-shRB cell proliferation (Fig. 3A,D), and triggered extensive cellular senescence in these cells (Fig. 3E-I). We also confirmed that cyclin D1 depletion was able to inhibit cell proliferation and to promote senescence in another RB-deficient cancer cell line TYBDC-1-shRB (Fig. 3J-L). Thus, the observation was not specific to only MCF7 cells.

We next established a pocket protein-deficient MCF7 cell line (MCF7-E7), in which all pocket proteins (RB, p107, p130) were destabilized by expression of HPV16 E7 (Helt and Galloway, 2001). We verified that MCF7-E7 cells were unresponsive to CDK4 inhibition and did not submit to senescence upon treatment with PD0332991 for 5 days (Fig. 3M,N). We found that cyclin D1 depletion effectively inhibited MCF7-E7 cell proliferation (Fig. 3O,P), and promoted widespread senescence in these pocket protein-deficient cells (Fig. 3Q).

Therefore, inhibition of CDK4 resulted in RB-mediated cellular senescence, but inhibition of cyclin D1 resulted in cellular senescence that was independent of RB.

Elevated ROS levels in cyclin D1-depleted cells trigger cancer cell senescence

Senescence could be triggered by various cellular stressors, including oxidative stress (Salama et al., 2014). To elucidate the cause of senescence associated with cyclin D1 depletion, we examined levels of reactive oxygen species (ROS) between the responders (cell lines that responded to cyclin D1 depletion by undergoing senescence: KKU-156, TYBDC-1, SKBR3, MCF7, KKU-214, UMSCC2), and the non-responders (cell lines that did not undergo senescence: MDA-MB-175, MDA-MB-134, T47D, ZR-75-1). Interestingly, there was a significant increase in endogenous ROS in all responder cell lines after cyclin D1 depletion, whereas no change in the level of endogenous ROS was observed in non-responder cell lines (Mann–Whitney *U*-test, P=0.0095) (Fig. 4A, left panel versus right panel). We noticed that the upregulation of ROS, and the senescence response were not related to average basal levels of ROS in each cell line (Fig. 4A, shcont). The upregulation of ROS was detected at approximately 48 h after cyclin D1 siRNA transfection, coinciding with cyclin D1 depletion, and it intensified at the 72 h time point (Fig. 4B,C). Interestingly, PD0332991 treatment, although resulting in cell cycle arrest and senescence, did not cause ROS elevation (Fig. S3A,B, and Fig. 4B).

To investigate whether the elevated ROS was responsible for the senescence phenotypes, we first induced the accumulation of ROS by treating MCF7 cells with H_2O_2. Many MCF7 cells responded to H_2O_2 treatment by undergoing senescence, suggesting that senescence is a primary response to oxidative stress in these cells (Fig. S4A). Next, we treated cyclin D1-depleted cells with the antioxidant *N*-acetylcysteine (NAC) to suppress intracellular ROS. We found that NAC treatment significantly reduced the number of cells that underwent senescence, gauged by SA-β-Gal and SAHF staining (Fig. 4D-F). NAC treatment did not reduce delayed senescence mediated by PD0332991 treatment, indicating that ROS plays a limited role in PD0332991-mediated senescence (Fig. S4B).

Of note, although NAC effectively suppressed senescence caused by cyclin D1 depletion, it was unable to entirely abolish the senescence (Fig. 4E,F). This suggested that senescence in cyclin D1-depleted cells may be influenced by a cause other than ROS. We and others have previously reported that cyclin D1 participates in homologous recombination (HR)-mediated DNA repair, and cyclin D1 depletion reduces the efficiency of HR (Li et al., 2010; Jirawatnotai et al., 2011). Reduced efficiency of HR may also contribute to cancer cell senescence observed in the cyclin D1-depleted cells. To this end, we employed a model cell line Capan-1, in which the HR is not functioning, because of a protein-truncating mutation in the *BRCA2* gene (Yuan et al., 1999). Therefore, in this cell line, we would be able to measure the antioxidative stress function of cyclin D1 without interference from the HR-related role of cyclin D1. We depleted cyclin D1 from Capan-1 and found that, cyclin D1 depletion resulted in increased senescence (Fig. S4C,D), suggesting an HR-independent anti-senescence role of cyclin D1. Next, we treated the cyclin D1-depleted cells with NAC and found that this abolished senescence to a level comparable with that in the control Capan-1 cells (Fig. S4C,D). Therefore, we believed that in the cells with normal HR, cyclin D1 plays a non-cell-cycle role to protect cells from senescence by facilitating efficient HR repair, and by keeping levels of intracellular oxidative stress at a tolerable sub-lethal level.

Cyclin D1 has been shown to negatively modulate the number of mitochondria, an important endogenous source of ROS (Sakamaki et al., 2006; Wang et al., 2006; Tchakarska et al., 2011). Consistent with previous reports, we found that cyclin D1-depleted cells exhibited an increased number of total and functioning mitochondria, as measured by transmission electron microscopy (TEM), expression of total mitochondria-specific DNA (*mtND5*) and MitoTracker staining (Fig. S4E-I).

We also measured the levels of mitochondrial superoxide using a specific fluoroprobe, MitoSOX, and detected an upregulation of the mitochondrial superoxide in cyclin D1-depleted cells, but not in cells treated with PD0332991 (Fig. S4J,K). An increase in total and functioning mitochondria was also found in RB-deficient cells, suggesting that the increase in ROS was independent of RB (Fig. S4L-P). This evidence collectively suggests that cancer cell senescence promoted by cyclin D1 depletion is mediated by ROS build-up in the cancer cells, which is possibly a consequence of the increased number of functioning mitochondria in the cells.

High levels of endogenous ROS activates the p38-FOXO3a-p27 pathway in cyclin D1-depleted cancer cells

To investigate the consequences of elevated ROS in cyclin D1-depleted cells, we studied the activation of p38 and JNK MAPK family proteins (hereafter p38 and JNK), which are involved in the oxidative stress response (Ho et al., 2012; Essers et al., 2004). We detected upregulation of phospho-p38 (Thr180/Tyr182) and JNK-mediated c-JUN phosphorylation at Ser73 in cyclin D1-depleted cells around 48-72 h after cyclin D1 depletion, but not in control cells (Fig. 5A, Fig. S5A). We did not detect activation of AKT in cyclin D1-depleted cells (Fig. S5B). Activation of p38 and JNK

Journal of Cell Science (2018) 131, jcs214726. doi:10.1242/jcs.214726

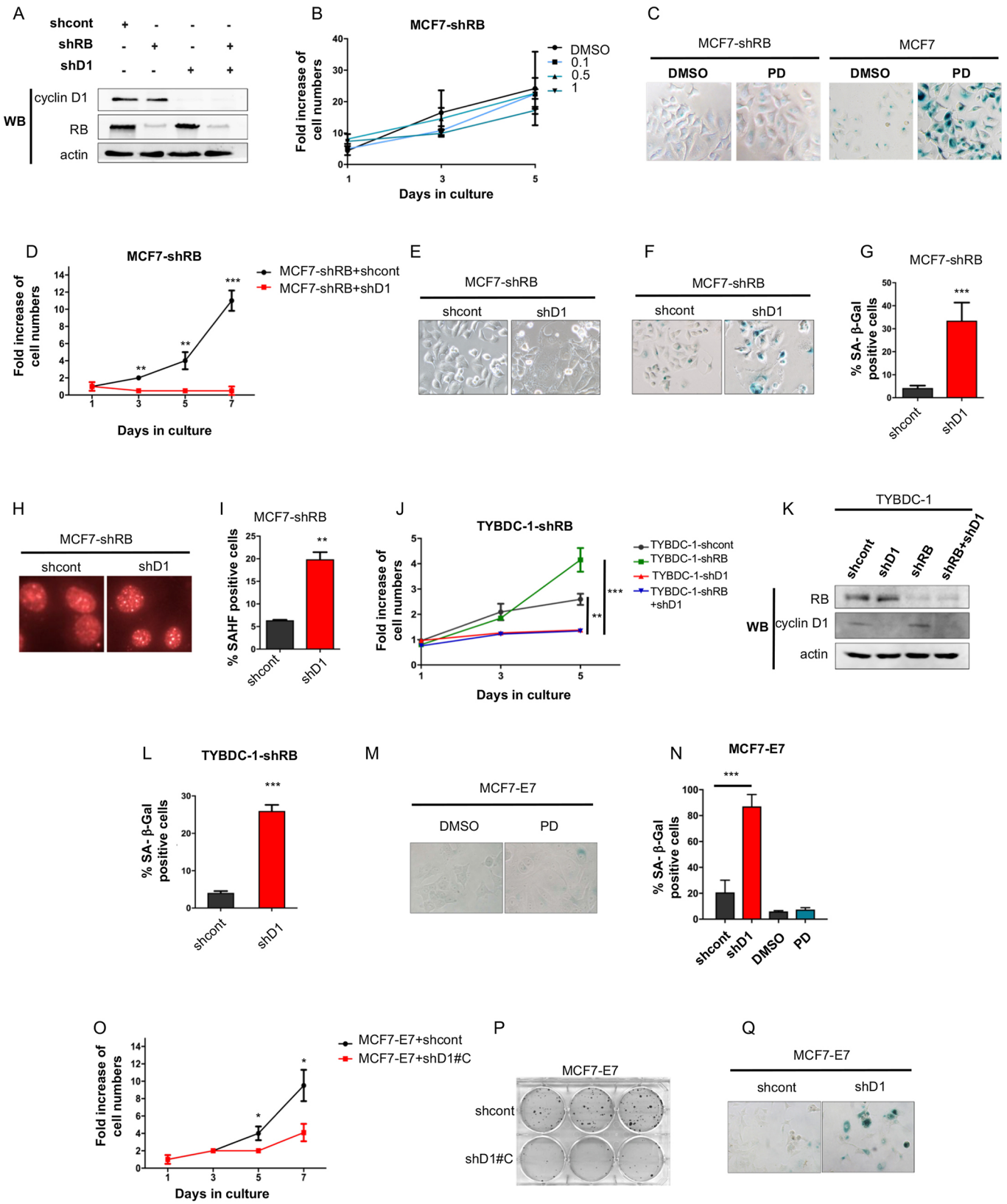

Fig. 3. See next page for legend.

was abolished, when cyclin D1-depleted cells were treated with NAC (Fig. 5B, Fig. S5C). FOXO3a is a transcription factor that activates genes in response to oxidative stress in order to mediate oxidative detoxification, cell cycle arrest and apoptosis. When it senses cellular stress, FOXO3a relocalizes to the nucleus and binds to promoters of target genes such as *SOD2* and catalase (Kops et al., 2002; Bartell et al., 2014). Where the stress level is overwhelming, FOXO3a can activate genes that promote senescence or apoptosis, such as

Journal of Cell Science (2018) 131, jcs214726. doi:10.1242/jcs.214726

Fig. 3. Senescence induced by depletion of cyclin D1 is independent of RB status. (A) Western blot (WB) analysis of cyclin D1 and retinoblastoma protein (RB) in MCF7 cells. Actin was used as a loading control. (B) Growth curves of MCF7 cells expressing RB-specific shRNA (MCF7-shRB) treated with indicated concentrations of PD0332991 (0.1, 0.5 or 1 µM) or vehicle (DMSO). (C) SA-β-Gal expression in MCF7-shRB cells was determined following a 5-day treatment with 0.5 µM PD0332991. MCF7 cells were used as a senescence control. (D) Growth curves of RB-deficient MCF7 cells expressing shcont or cyclin D1-specific shRNA (shD1#C). (E) Cellular morphology and (F) SA-β-Gal expression of MCF7-shRB cells with non-targeting (shcont) or shD1. (G) Mean percentage ±s.d. of SA-β-Gal-positive cells from F. (H,I) Immunofluorescence (H) and analysis (I) of SAHF in cyclin D1-depleted MCF7-shRB cells. (J) Growth curves of TYBDC-1 expressing non-targeting shRNA control (shcont; gray), RB-specific shRNA (shRB; green), cyclin D1-specific shRNA (shD1#C; red), and shRB+shD1 (purple). Statistical significance was determined by two-way ANOVA (**$P \leq 0.01$, shcont vs shD1; ***$P \leq 0.001$, shRB vs shRB+shD1). (K) WB analysis of cyclin D1 and retinoblastoma protein (RB) in RB-deficient TYBDC-1 cells expressing shcont, or shD1. (L) Mean percentage ±s.d. of SA-β-Gal-positive cells in RB-deficient TYBDC-1 cells expressing shcont, or shD1. (M) SA-β-Gal expression in DMSO and PD0332991 (PD)-treated E7-expressing MCF7 cells (MCF7-E7) at day 5 after treatment. (N) Percentages of SA-β-Gal-positive cells were determined after MCF7-E7 was transduced with the indicated shRNAs (shcont or shD1), or treated with DMSO or PD0332991. (O) Growth curves of MCF7-E7 cells expressing either shcont or shD1 (shD1#C). (P) Colony-forming assay of MCF7-E7 cells expressing shcont or shD1 (shD1#C). (Q) SA-β-Gal expression in MCF7-E7 expressing shcont or shD1 cells. Bars represent averages of three independent experiments. Statistical significance was determined with Student's *t*-test (*$P \leq 0.05$, **$P \leq 0.01$ and ***$P \leq 0.001$).

CDKN1B (encoding the cell cycle inhibitor p27) or *GADD45A* and *BIM* (Lam et al., 2013).

We detected an upregulation of FOXO3a protein in association with increased FOXO3a Ser7 phosphorylation, which is involved in the stress-induced activation of FOXO3a by p38 (Ho et al., 2012) (Fig. 6A,B) and translocalization of FOXO3a from the cytoplasm to the nucleus after cyclin D1 depletion (Fig. 6C-E). This translocalization of FOXO3a was abolished by NAC treatment (Fig. S5D), indicating that the translocalization was associated with ROS. We detected recruitment of endogenous FOXO3a to promoters of several downstream genes, such as *CDKN1B*, *SOD2*, *GADD45a*, *PrxIII* and *BCL10*, by FOXO3a chromatin immunoprecipitation (Fig. S6) in cyclin D1-depleted cells. Activation of FOXO3a was also detected when cyclin D1 was depleted in RB-deficient MCF7 cells (Fig. 6E). We confirmed the activation of FOXO3a by cyclin D1 depletion in cell lines TYBDC-1 and KKU-214 (Fig. 6F). Lastly, we detected upregulation of several genes known to be regulated by FOXO3a (Fig. 6G). Therefore, cyclin D1 depletion was sufficient to fully activate FOXO3a. Together, these results confirmed that the activation of FOXO3a is induced by ROS in cyclin D1-depleted cells.

To elucidate the cause of RB-independent cellular senescence in cyclin D1-depleted cells, we focused on upregulated p27 (encoded by *CDKN1B*), since it is a gene downstream of FOXO3a known to regulate cellular senescence through multiple mechanisms, including RB-independent mechanisms (Majumder et al., 2008; Young et al., 2008). We found that p27 protein level was also upregulated in cyclin D1-depleted cells (Fig. 6H), whereas GADD45a and SOD2 were not upregulated at the protein level (Fig. S7A). The upregulation of p27 coincided with p38 and c-JUN phosphorylation (Fig. S7B). In addition, we detected increased binding between p27 and CDK2 in cyclin D1-depleted cells by CDK2 immunoprecipitation, implying an increased p27 function (Fig. S7C). We measured senescence levels in MCF7 and MCF7-shRB cells co-transfected with siRNAs against cyclin D1 and p27. We found that p27 siRNA significantly increased the number of EdU-positive cells, and reduced the number of SAHF-positive cells in both cyclin D1-depleted MCF7 and MCF7-shRB cells, indicating that p27 depletion prevents the cell cycle arrest and senescence observed in cyclin D1-depleted cells (Fig. 6I-L). Therefore, p27 mediates, at least partially, the cell cycle arrest and cellular senescence found in cyclin D1-depleted cells.

DISCUSSION

Overexpression of cyclin D1 is commonly found in many types of cancer. However, precisely how overexpressed cyclin D1 contributes to cancer formation is not entirely known. In this study, we investigated a novel anti-senescence role of cyclin D1 in human cancer. We found that cyclin D1 expression maintains endogenous ROS at a sub-lethal level, likely by inhibiting the number and function of mitochondria. In the absence of cyclin D1, cancer cells accumulate intolerable levels of endogenous ROS, which subsequently triggers cancer cell senescence and possibly cell death. The senescence triggered by cyclin D1 depletion appeared to be independent of the cell cycle regulatory function of cyclin D1, since the senescence induced by cyclin D1 depletion fully occurred in RB-deficient cells. In addition, ROS-induced senescence was specific to cyclin D1 depletion, and was not observed in cells treated with a CDK4/6-specific inhibitor. We, therefore, conclude that cyclin D1 has a CDK4- and RB-independent role in maintaining oxidative balance in the cancer cells. This novel function, along other cancer-promoting functions such as function in HR, makes cyclin D1 a multifunctional oncoprotein that facilitates overall cancer cell survival (Fig. 7A).

We elucidated that the senescence was mediated by the p38-JNK-FOXO3a-p27 pathway, which was activated by elevated ROS after cyclin D1 depletion (Fig. 7B). FOXO3a is a tumor suppressor, which facilitates apoptosis and senescence upon stress (Nestal de Moraes et al., 2016). It was shown that FOXO3a functions at both transcriptional and post-transcriptional levels to promote p27 expression (Lam et al., 2013; Wu et al., 2013). p27 is a CDK2 inhibitor, capable of blocking non-RB processes of cell division controlled by CDK2 (Chae et al., 2004; Luscher-Firzlaff et al., 2006; Voit et al., 1999). We found that a higher amount of p27 was co-precipitated with CDK2 in cyclin D1-depleted cells, promoting a downregulation of CDK2 activity. This finding suggested that p27 may be a key regulator for senescence in cyclin D1-depleted cells. We have also examined the expression of *GADD45A* and *SOD2*, downstream genes of FOXO3a, which are also involved in senescence. Although, in cyclin D1-depleted cells, FOXO3a localized at the promoters of *GADD45A* and *SOD2* (Fig. S6) and the mRNAs were upregulated (Fig. 6G), we found that GADD45A and SOD were not upregulated at the protein level (both in RB-negative and RB-positive cells). From these results, we believe that the role of GADD45A and SOD2 might be limited in this context. Although we found that depletion of p27 significantly suppressed senescence, it is possible that there are other FOXO3a target genes that also contribute to the senescence induced by cyclin D1 depletion.

Previous studies demonstrated that cyclin D1 represses mitochondria number and that cyclin D1 functions by two possible mechanisms. First, cyclin D1 and CDK4 phosphorylates and represses nuclear respiratory factor-1 (NRF-1), a transcription factor that induces nuclear-encoded mitochondrial genes (Wang et al., 2006). Second, cyclin D1, independently of CDK4, competes with hexokinase 2 to bind to a voltage-dependent anion channel and inhibit mitochondrial function (Tchakarska et al., 2011). However, the biological role of these findings in diseases such as cancer is not

Journal of Cell Science (2018) 131, jcs214726. doi:10.1242/jcs.214726

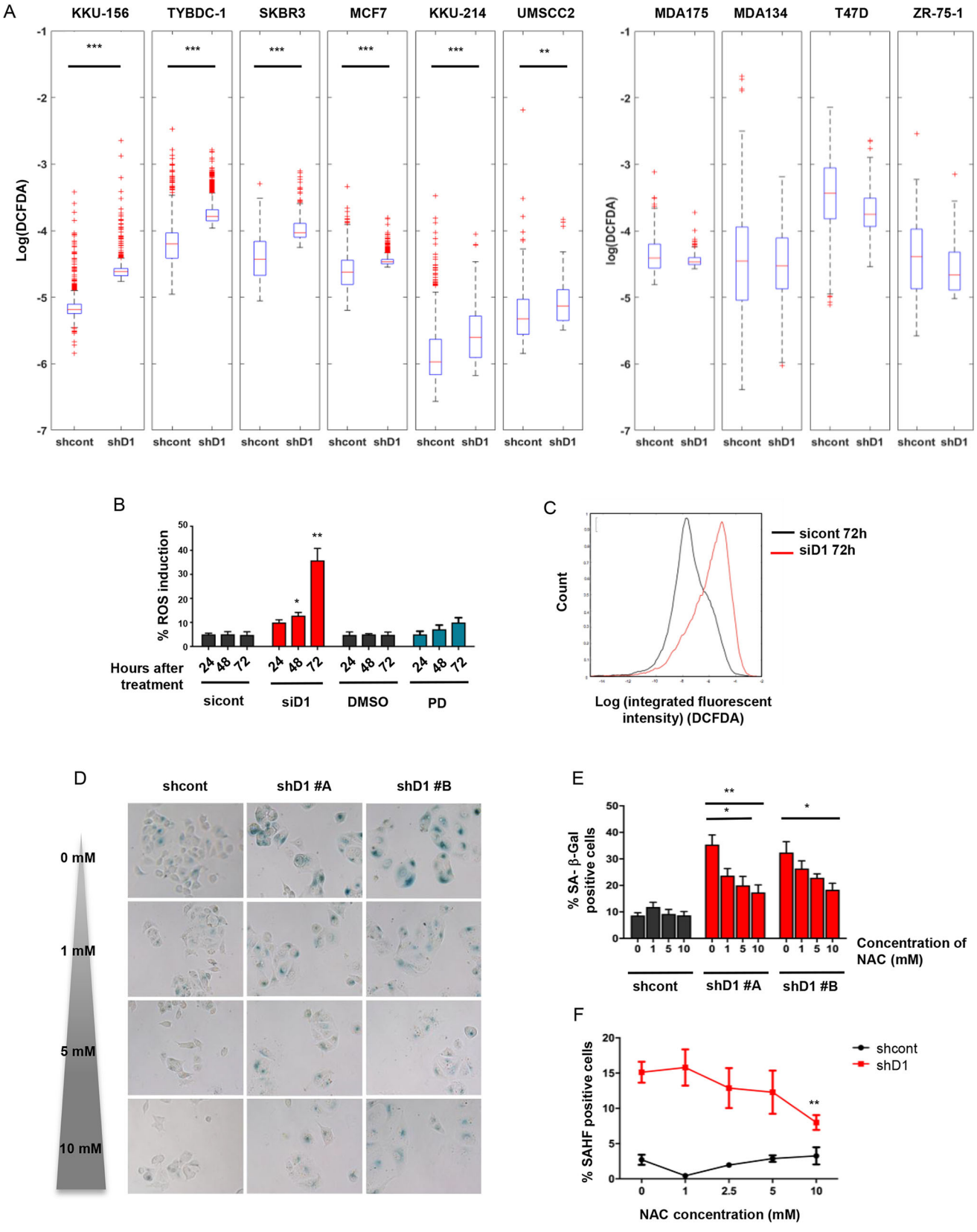

Fig. 4. See next page for legend.

entirely clear. Our results demonstrated that, in addition to the role of cyclin D1 in cell cycle control, a new role of cyclin D1 in maintaining oxidative balance is critical for RB-positive and RB-negative cancer cells to survive. It remains to be addressed why some cancer cells managed to avoid ROS accumulation and thus escaped senescence, upon cyclin D1 depletion. These cells may

Journal of Cell Science (2018) 131, jcs214726. doi:10.1242/jcs.214726

Fig. 4. Reactive oxygen species (ROS) are upregulated in cyclin D1-depleted cancer cells and are responsible for senescence. (A) Cancer cells were transduced with lentivirus expressing either non-targeting shRNA (shcont) or cyclin D1-specific shRNA (shD1). After 4 days, ROS levels were measured using carboxy-DCFDA. Box plots show distributions of ROS in the indicated cell lines. Statistical significance was determined by Mann–Whitney *U*-test. Box shows median (red line) and 25th and 75th percentiles, respectively. Whiskers are extended to the most extreme data points not considered outliers, and the outliers are plotted individually using the '+' symbol. (B) ROS levels measured in MCF7 cells transfected with non-targeting siRNA (sicont) or cyclin D1 siRNA (siD1), or treated with vehicle (DMSO) or PD0332991 (PD) at indicated time points (24, 48, and 72 h). Bars represent average percentages of DCFDA-positive cells ±s.d. (C) Histograms of intracellular ROS levels in MCF7 cells transfected with sicont or siD1 at 72 h post-transfection. At least 500 DCFDA-positive cells were analyzed. (D) SA-β-Gal expression in cyclin D1-depleted MCF7 cells treated with indicated NAC concentrations. (E) Quantification of SA-β-Gal-positive cells after treatment with indicated concentrations of NAC. Bars represent average percentages of positive cells ±s.d. (F) Percentages of SAHF-positive cells after NAC treatment. Statistical significance was determined with Student's *t*-test (*$P \leq 0.05$, **$P \leq 0.01$ and ***$P \leq 0.001$).

rely on a different type of redox modulation to cope with the consequences of excessive ROS.

Control of the cell cycle and cellular energy level have been shown to be coordinated. Disruption of the energy balance may disrupt the normal cell cycle and vice versa (Salazar-Roa and Malumbres, 2017). Thus, it may be sensible when a cell cycle machinery component such as cyclin D1 also plays a dual role in controlling energy and oxidative balance during cell cycle. Cancer cells do not invent new pathways for survival, but instead use pre-existing machineries to operate. Consequently, they may become reliant on this adaptation. Our findings offer a view of cyclin D1 as a regulator that controls the cancerous oxidative balance, and describe the consequences when this balance is altered by cyclin D1 depletion. The role of cyclin D1 in other contexts and settings requires further investigation.

Altered redox status has long been observed in cancer cells. This adopted property of cancer cells can be exploited for therapeutic benefits (Trachootham et al., 2009) and we propose that inhibition of cyclin D1 may make cancer cells hypersensitive to such ROS-modulating agents.

MATERIALS AND METHODS

Cell culture and treatment

The MDA-MB-175, ZR-75-1, MDA-MB-134, T47D, SKBR3, and MCF7 cell lines were from ATCC (Manassas, VA, USA). UMSCC2 was from University of Michigan cell bank. KKU-156, KKU-214 and TYBDC-1 cell lines were from the Japanese Collection of Research Bioresources (JCRB) Cell Bank (Osaka, Japan). Cell line authentication was done by short tandem repeat (STR) profiling at the cell line banks indicated. The MDA-MB-175, ZR-75-1, and T47D were maintained in RPMI1640; SKBR3 in McCoy's 5A Medium; MDA-MB-134 in L-15; and MCF7, UMSCC2, KKU-156, KKU-214, and TYBDC-1 in DMEM, supplemented with 10% FBS and 100 U/ml penicillin-streptomycin under standard conditions. shRNA-expressing cells were maintained in selection medium with one of the antibiotics, puromycin, G418 or hygromycin (Thermo Fisher Scientific, MA, USA). NAC was from Amresco (Solon, OH, USA). PD0332991 was a gift from Piotr Sicinski, Dana Farber Cancer Institute (DFCI), Boston, MA, USA. Carboxy-H2DCFDA was from Sigma-Aldrich (St Louis, MO, USA; D6883).

Plasmids and siRNA

The shD1-pLKO.1#A(5′-GCCAGGATGATAAGTTCCTTT-3′), #B (5′-ATTGGAATAGCTTCTGGAAT-3′), and a control non-targeting shRNA (5′-CAACAAGATGAAGAGCACCAA-3′) (each contains puromycin resistance gene) were from Sigma-Aldrich. The cyclin D1-shRNA (pBabe-neo) #C (5′-CCACAGATGTGAAGTTCATTT-3′) [contains a neomycin (geneticin) resistance gene], was a gift from Ewa Sicinska, DFCI. The pGIPZ *RB1*-shRNA (5′-CGCAGTTCGATATCTAC-TGAAA-3′) was provided by Sunkyu Kim, Novartis Institutes for Biomedical Research. pBabe-hygro-E7 was provided by Denise Galloway, Fred Hutchinson Cancer Research Center, Seattle, WA, USA. pRc/CMV-cyclin D1 K112E-HA was from Addgene (plasmid #8952, deposited by Philip Hinds). The pcDNA plasmid was purchased from Invitrogen. Cyclin D1-specific siRNAs (SI02654547), CDK4 (SI00604744) and control siRNA (1027310) were from Qiagen (Valencia, CA, USA). Cyclin D1-UTR targeted siRNA used in K112E experiment (#s229) was from Thermo Fisher Scientific (MA, USA). The p27 siRNA (sc-29429) was from Santa Cruz Biotechnology (Santa Cruz, CA, USA).

Cyclin D1 re-expression in senescent cells and expression of K112E cyclin D1

The inducible system (Takara Bio Inc., Mountain View, CA, USA), composed of pEF1α-Tet3G and pTRE3G-cyclin D1-HA plasmids was co-transfected with GFP-expressing plasmid peGFP (a gift from Piotr Sicinski, DFCI) into MCF7 cells, followed by cyclin D1 depletion using cyclin D1-specific shRNA targeting the 5′UTR of cyclin D1 mRNA (shD1#A). Expression of cyclin D1-HA was achieved by addition of 1 µM doxycycline. Analyses of SAHF and EdU-positive cells were performed in cells expressing cyclin D1-HA (GFP-expressing cells) by immunofluorescence 48 h after doxycycline induction. The pRc/CMV-K112E-cyclin D1 was transiently co-transfected with peGFP to MCF7 cells for 24 h, then the cells were transfected with non-targeting siRNA or cyclin D1-UTR targeted siRNA. Seventy-two hours after siRNA transfection, cells were fixed and GFP-expressing cells were analyzed for SAHF.

Detection of DNA damage

Cells were transduced with non-targeted shRNA control or cyclin D1-specific shRNA. After 4 days, γH2AX foci were analyzed as described previously (Jirawatnotai et al., 2011).

Growth and colony-forming assays

For growth curves, cells were seeded into 24-well plates at a density of 5000 cells/well. Cell numbers were counted at indicated time points. For colony-forming assays, 200 cells/well were seeded into 6-well plates. After 14 days, colonies were fixed with 10% neutral buffered formalin for 30 min and stained with 0.5% Crystal Violet solution for visualization.

SA-β-gal assay

SA-β-gal assay was performed as previously described (Debacq-Chainiaux et al., 2009). The percentage of SA-β-gal-positive cells was calculated from at least 500 cells.

Semi-quantitative real-time PCR

Total RNA was extracted using an RNA extraction kit (Thermo Fisher Scientific). Complementary DNA was generated by Superscript III reverse transcriptase and oligo-dT primers (Thermo Fisher Scientific). Transcript levels were normalized to expression of *GAPDH*. The mitochondrial DNA (mtDNA), *mtND5* was analyzed against *HBB*. All primers used in this experiment were synthesized by bioDesign, Bangkok, Thailand. The primers used were: p16-for: 5′-CCGAATAGTTACGGTCGGAGG-3′, p16-rev: 5′-CACCAGCGTGTCCAGGAAG-3′; *LMNB1*-for: 5′-AGCGG-AAGAGGGTTGATGTG-3′, *LMNB1*-rev: 5′-CCAGCCTCCCATTGGT-TGAT-3′; *mtND5*-for: 5′-GCCTAGCATTAGCAGGAATAC-3′, *mtND5*-rev: 5′-GGGGAAGCGAGGTTGACCTG-3′; *HBB*-for: 5′-GCTTCTGAC-ACAACTGTGTTCACTAGC-3′, *HBB*-rev: 5′-CACCAACTTCATCCAC-GTTCACC-3′; *GADD45A*-for: 5′-TCCTGCTCTTGGAGACCGA-3′, *GADD45A*-rev: 5′-ATCCATGTAGCGACTTTCCCG-3′; *BIM*-for: 5′-CA-AGAGTTGCGGCGTATTGG-3′, *BIM*-rev: 5′-TGTCTGCATGGTATCT-CGGC-3′; *SOD2*-for: 5′-TGGCCAAGGGAGATGTTACAG-3′, *SOD2*-rev: 5′-CTTCCAGCAACTCCCCTTTG-3′; *p27*-for: 5′-TCTGAGGACA-CGCATTTGGT-3′, *p27*-rev: 5′-ACAGAACCGGCATTTGGGG-3′; *GAPDH*-for: 5′-CCTCCAAAATCAAGTGGGGCGATG-3′, *GAPDH*-rev: 5′-CGAACATGGGGGCATCAGCAGA-3′.

Journal of Cell Science (2018) 131, jcs214726. doi:10.1242/jcs.214726

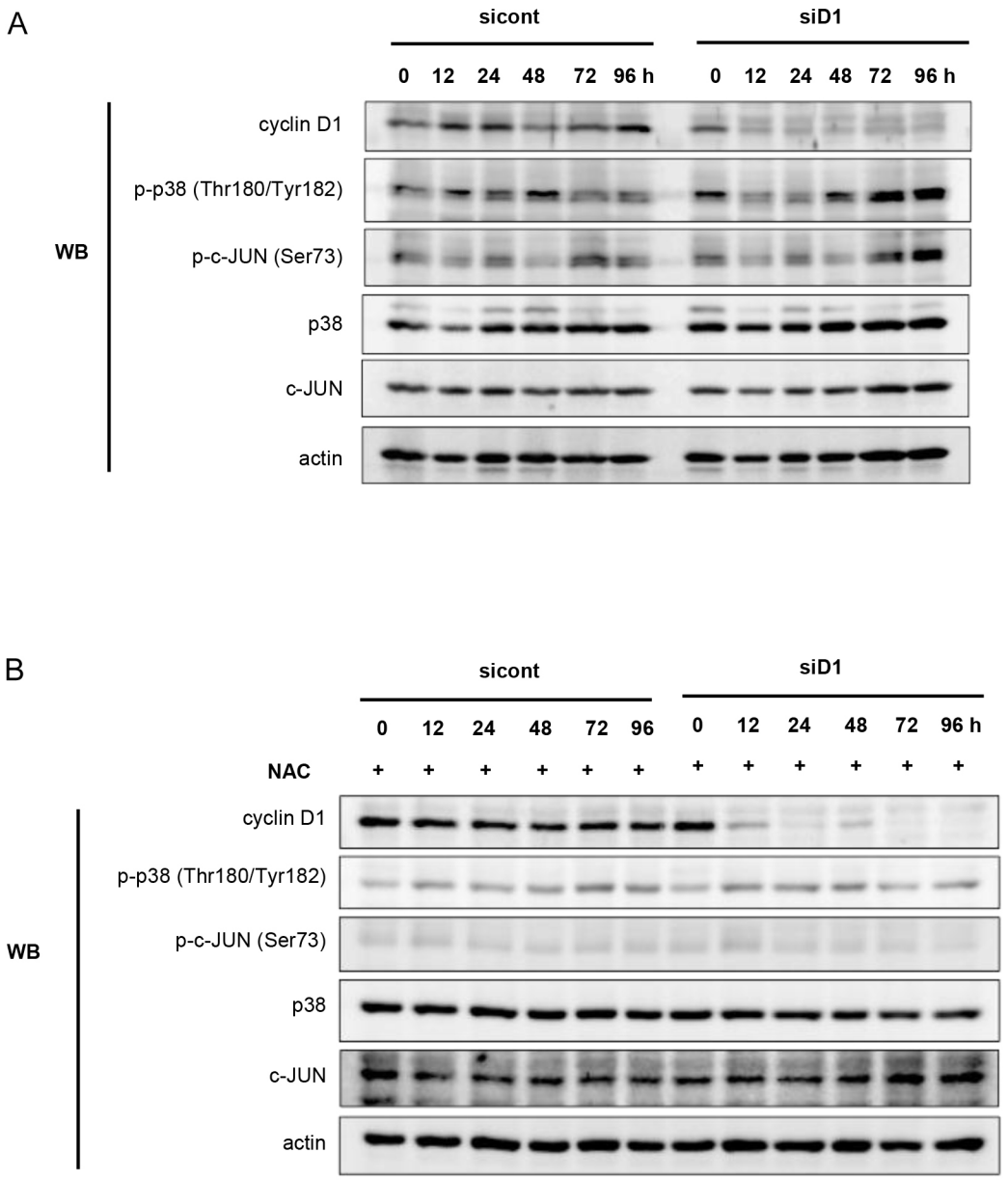

Fig. 5. Upregulation of ROS in cyclin D1-depleted cells activates p38 and JNK pathways. Western blot (WB) analysis of p38 and c-JUN activation. (A) Protein lysates were prepared at 0, 12, 24, 48, 72, and 96 h after non-targeted siRNA (sicont) or cyclin D1 siRNA (siD1) transfection. (B) WB analysis was performed as in A, except that freshly prepared NAC was added to the cells every other day from 0 h until the cells were harvested.

Apoptosis detection

Cells were analyzed for apoptosis using an Annexin-V Apoptosis Detection Kit according to the manufacturer's instructions (Thermo Fisher Scientific). Forty-eight hours after siRNA transfection, 10,000 cells from each condition were analyzed by flow cytometry (CytoFLEX, Beckman Coulter, Brea, CA, USA).

ROS measurement

ROS measurement was performed in 96-well plates. Cells were seeded at a density of 8×10^3 cells/well. At the detection time, cells were washed twice with PBS, and carboxy-DCFDA dye in serum-free medium was added at a final concentration of 5 µM. Plates were incubated at 37°C for 30 min, before removal of the dye. Cells were then washed twice with PBS, stained with nuclear staining dye and immediately analyzed with a high-content imaging system (PerkinElmer, Bangkok, Thailand). Results are presented as a median fluorescent intensity. For mitochondrial-specific superoxide detection, cells were transduced with either non-targeting shRNA (shcont) or cyclin D1-specific shRNA. After 4 days, cells were incubated with MitoSOX Red (Thermo Fisher Scientific), fixed and counterstained with DAPI, according to the manufacturer's instructions. Mean integrated fluorescence intensities were analyzed using a high-content imaging system.

Western blotting and immunoprecipitation

Western blotting and immunoprecipitation were performed as previously described (Jirawatnotai et al., 2011) using specific antibodies.

Immunofluorescence staining

Cells were seeded in microplates (#3904) (Corning, Corning, NY, USA) and fixed in 4% paraformaldehyde, permeabilized in methanol, and blocked in Odyssey Blocking Buffer (PBS) (LI-COR, Lincoln, NE, USA). Cells were then incubated with specific primary antibody overnight, followed by 1:1000 dilution fluorescent-conjugated secondary antibody prior to nuclear staining with DAPI. For detection of cells in S-phase, cells were pulsed with EdU (5-ethynyl-2-deoxyuridine) for 90 min, fixed and stained by Click-iT

Journal of Cell Science (2018) 131, jcs214726. doi:10.1242/jcs.214726

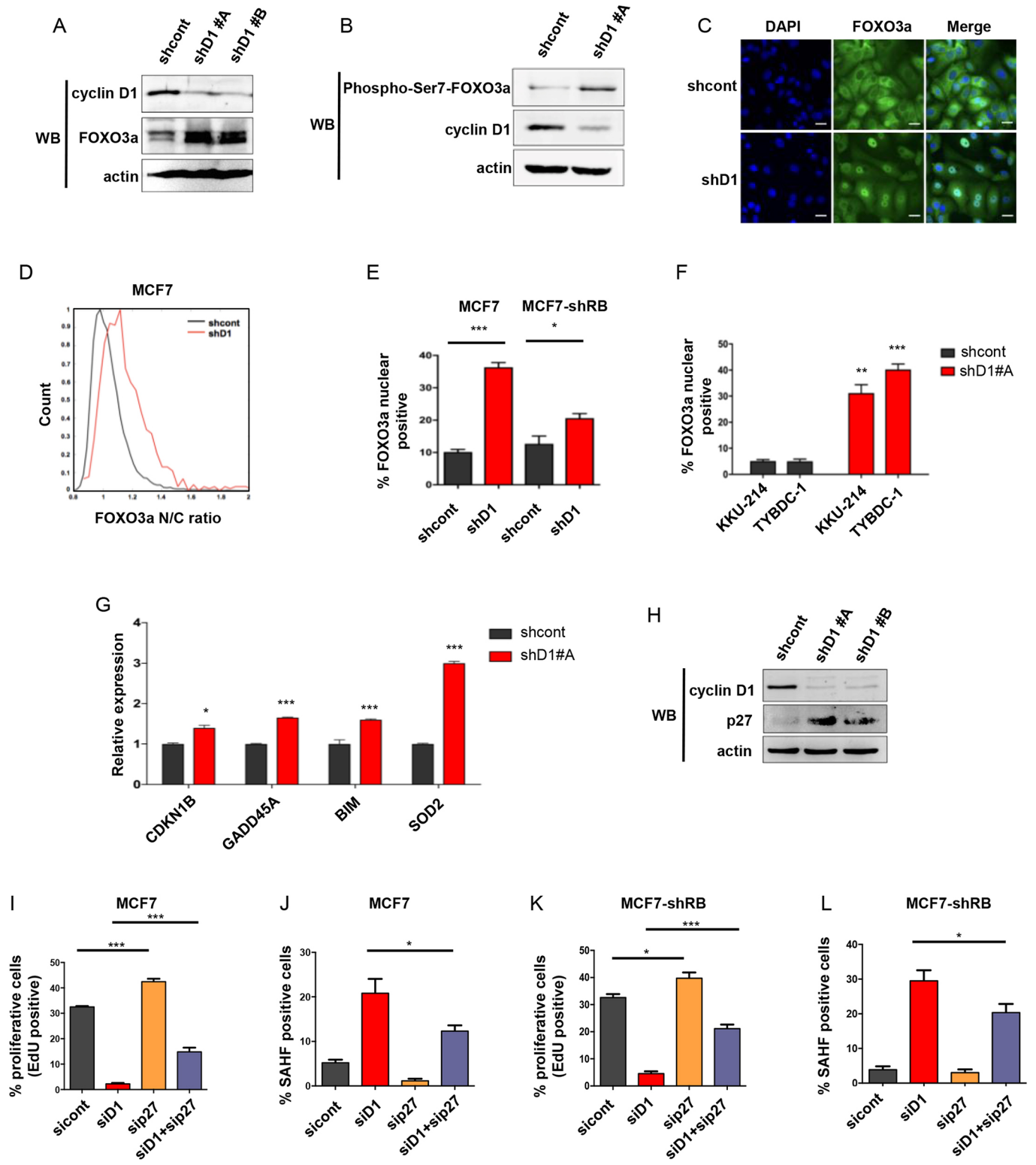

Fig. 6. See next page for legend.

reaction according to the manufacturer's protocol (C10337) (Thermo Fisher Scientific). Samples were evaluated by the high-content imaging system.

Mitochondrial staining

Cells were stained with 250 nM MitoTracker Red CMXRos (#9082) (Cell Signaling, Danvers, MA, USA) and DAPI before assessment in the high-content imaging system.

Chromatin immunoprecipitation (ChIP)

MCF7 cells were transduced with either non-targeting control shRNA (shcont) or cyclin D1-specific shRNA (shD1) for 4 days. Chromatin immunoprecipitation was performed as described earlier (Jirawatnotai et al., 2011). Briefly, samples were immunoprecipitated overnight at 4°C with anti-FOXO3a ChIP grade antibody. The immune complexes were captured using Protein G beads (Santa Cruz). After a series of washing steps, the

Journal of Cell Science (2018) 131, jcs214726. doi:10.1242/jcs.214726

Fig. 6. Elevated ROS induces hyper-functional FOXO3a. (A) Western blot (WB) analysis of total FOXO3a in MCF7 cells expressing non-targeting shRNA (shcont) or cyclin D1 shRNA (shD1). (B) WB analysis of phospho-Ser7 FOXO3a in MCF7 cells expressing shcont or shD1. Actin was used as a loading control. (C) Immunofluorescence of FOXO3a localization (green) in cyclin D1-depleted MCF7 cells. Nuclei were counterstained with DAPI (blue). Scale bars: 5 µm. (D) Histograms of FOXO3a nuclear-to-cytoplasmic (N/C) ratio shows intracellular distribution of FOXO3a in MCF7 cells expressing shcont (black) compared with shD1 (red). (E) Percentage of FOXO3a-nuclear-positive in MCF7 and MCF7-shRB cells. (F) Percentage of FOXO3a nuclear-positive KKU-214 and TYBDC-1 cells, after cyclin D1 depletion. The nuclear FOXO3a-positive cells were counted from a total of at least 5000 cells. (G) Expression of *CDKN1B* (p27), *GADD45A*, *BIM* and *SOD2* genes was determined by qRT-PCR. The mRNAs were harvested after cyclin D1 depletion in MCF7 cells. Bars represent mean±s.d. (H) WB analysis of p27 protein expressions in cyclin D1-depleted cells. (I) Analysis of proliferative cells by 5-ethynyl-2′-deoxyuridine (EdU) incorporation and (J) percentage of SAHF-positive cells in MCF7 transfected with sicont, siD1, or sip27, as indicated. Analyses of proliferative cells by 5-ethynyl-2′-deoxyuridine (EdU) incorporation (K) and percentage of SAHF-positive cells in MCF7-shRB cells (L) transfected with sicont, siD1, sip27, as indicated. Bars represent averages of three independent experiments. Statistical significance was determined with Student's *t*-test (**P*≤0.05, ***P*≤0.01, and ****P*≤0.001).

beads were extracted in 120 µl of elution buffer (0.1 M $NaHCO_3$, 1% SDS) and analyzed by qPCR. Primers used for PCR amplification (5′ to 3′) were as follows: p27 F, CAACCAATGGATCTCCTCCT, p27 R, GCCTCTCT-CGCACTCTCAAA; BCL10 F, AAGCTGCAGTGAGCCGAGAA, BCL10 R, TAGGGCTGCCGGGATCATA; PrxIII F, CGGACTAAAAC-TGCATTTGTAATTA, PrxIII R, CACGTGGTTTTCCTACTGTC; MnSOD F, GTTCCTCTTCGCCTGACTGTT, MnSOD R, CTGAACCG-TTTCCGTTGCTT; GADD45A F, CACTCTCGGGACTTCTCACG, GADD45A R, GCACCTGGGCTCTACGAAAA.

Antibodies

Rabbit anti-cyclin D1 (sc-753), mouse anti-actin (sc-47778), mouse anti-HSP90 (sc-13119), mouse anti-total p38 (sc-535), mouse anti-total c-JUN (sc-74543), mouse anti-GADD45 (sc-6850), and mouse anti-Cdk2 (sc-6248) were purchased from Santa Cruz Biotechnology. Rabbit anti-FOXO3a (07-702), rabbit anti-trimethyl-histoneH3 (Lys9); H3K9 (07-442), mouse anti-γH2AX Ser139 (05-636), and mouse anti-SOD2 (MAB4081) were purchased from Merck Millipore (Bangkok, Thailand). Rabbit anti-FOXO3a (#2497), mouse anti-Rb (#9309), rabbit anti-phospho-p38 (Thr180/Tyr182, #4511), rabbit anti-phospho-c-JUN (Ser73, #3270), rabbit anti-phospho-AKT (Ser473, #4060), rabbit anti-phospho-FOXO3a (Ser7, #14724S) were from Cell Signaling. The rabbit anti-FOXO3a ChIP-grade (ab12162) was from Abcam, UK. All antibodies were used at 1:500 for immunoprecipitation, 1:1000 for western blotting and 1:300 for immunofluorescence staining.

Transmission electron microscopy (TEM)

Sample preparation and analyses were performed according to a standard method as previously described (Parameyong et al., 2013).

Image processing and analysis

All images from the high-content imaging system were analyzed using Columbus Image Data Storage and Analysis System (PerkinElmer), CellProfiler 2.1.1 and MATLAB R2015b. ImageStudio program was used for quantification of western blot signals.

Statistical analysis

The Mann–Whitney *U*-test was used to evaluate significance between the median of control (shcont) and the cyclin D1 knockdown groups (shD1) in ROS measurement analysis and to compare ROS changes in the non-responder versus the responder group; changes in ROS from all cell lines in each group were calculated from the median values. Comparison between

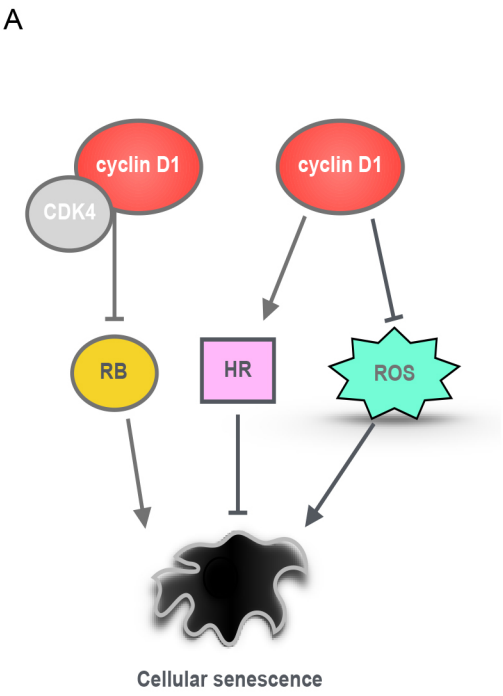

Fig. 7. Anti-senescence role of cyclin D1 in cancer cells. (A) Cyclin D1 is required for cancer cell survival and proliferation by promoting cell cycle entry and efficient homologous recombination (HR)-mediated DNA repair. Cancer cells are known to have a high level of oxygen consumption and thus adopt vigorous oxidative stress defense mechanisms (Ward and Thompson, 2012). We show that cyclin D1 also has an additional role in maintaining reactive oxygen species (ROS) at a sub-lethal level (right). (B) Depletion of cyclin D1 overwhelms cancer cells with increased level of ROS. Consequently, elevated ROS signal via several intracellular pathways, including p38-JNK-FOXO3a-p27 to promote cancer cell senescence.

groups of cell numbers in the TYBDC-1 experiment was performed using a two-way ANOVA. Comparison between two groups was performed using two-tailed Student's *t*-test, except where another method is specified. Experiments were performed in biological triplicates. The positive SA-β-Gal cells were counted from at least 500 cells. Positive SAHF and proliferative cells were counted in a total number of at least 3000 cells. The numbers of samples in other experiments are specified. Bars represent the mean±s.d. The level of statistical significance was determined as $*P \leq 0.05$, $**P \leq 0.01$ and $***P \leq 0.001$.

Acknowledgements
We thank Dr Sunkyu Kim, Novartis Institutes for Biomedical Research, Cambridge, MA, for RB-specific shRNA. We would like to thank Drs Piotr Sicinski (DFCI), Nont Kosaisawe and Bhoom Suktitipat (Siriraj Hospital) for their advice.

Competing interests
The authors declare no competing or financial interests.

Author contributions
Conceptualization: S.J.; Methodology: P. Laphanuwat, P. Likasitwatanakul, G.S., N.C., K.C., U.P., S.S.; Formal analysis: P. Laphanuwat, G.S.; Investigation: P. Laphanuwat, P. Likasitwatanakul, G.S., A.T., N.C., N.K., S.J.; Resources: O.S., K.C., E.W.-F.L., S.O., S.S., S.J.; Data curation: P. Laphanuwat; Writing - original draft: S.J.; Writing - review & editing: P. Laphanuwat, S.J.; Supervision: S.J.; Project administration: S.J.; Funding acquisition: S.J.

Funding
This study was supported by the Thailand Research Fund [RSA5880038]; Siriraj Research Fund; The Foundation for Cancer Care, Siriraj Hospital, and the Advanced Research on Pharmacology Fund; Siriraj Foundation [D003421]. S.J., U.P. and S.S. are supported by the Chalermphrakiat Grant, Faculty of Medicine Siriraj Hospital, Mahidol University. E.W.-F.L. is supported by the Medical Research Council [MR/N012097/1]; Cancer Research UK [A12011]; Breast Cancer Now [2012MayPR070; 2012NovPhD016]; and the CRUK Imperial Centre.

Supplementary information
Supplementary information available online at
http://jcs.biologists.org/lookup/doi/10.1242/jcs.214726.supplemental

References
Bartell, S. M., Kim, H.-N., Ambrogini, E., Han, L., Iyer, S., Serra Ucer, S., Rabinovitch, P., Jilka, R. L., Weinstein, R. S., Zhao, H. et al. (2014). FoxO proteins restrain osteoclastogenesis and bone resorption by attenuating H2O2 accumulation. *Nat. Commun.* **5**, 3773.

Brown, N. E., Jeselsohn, R., Bihani, T., Hu, M. G., Foltopoulou, P., Kuperwasser, C. and Hinds, P. W. (2012). Cyclin D1 activity regulates autophagy and senescence in the mammary epithelium. *Cancer Res.* **72**, 6477-6489.

Casimiro, M. C. and Pestell, R. G. (2012). Cyclin d1 induces chromosomal instability. *Oncotarget* **3**, 224-225.

Chae, H. D., Yun, J., Bang, Y. J. and Shin, D. Y. (2004). Cdk2-dependent phosphorylation of the NF-Y transcription factor is essential for the expression of the cell cycle-regulatory genes and cell cycle G1/S and G2/M transitions. *Oncogene* **23**, 4084-4088.

Choi, Y. J., Li, X., Hydbring, P., Sanda, T., Stefano, J., Christie, A. L., Signoretti, S., Look, A. T., Kung, A. L., von Boehmer, H. et al. (2012). The requirement for cyclin D function in tumor maintenance. *Cancer Cell* **22**, 438-451.

Debacq-Chainiaux, F., Erusalimsky, J. D., Campisi, J. and Toussaint, O. (2009). Protocols to detect senescence-associated beta-galactosidase (SA-betagal) activity, a biomarker of senescent cells in culture and in vivo. *Nat. Protoc.* **4**, 1798-1806.

Essers, M. A. G., Weijzen, S., de Vries-Smits, A. M. M., Saarloos, I., de Ruiter, N. D., Bos, J. L. and Burgering, B. M. T. (2004). FOXO transcription factor activation by oxidative stress mediated by the small GTPase Ral and JNK. *EMBO J.* **23**, 4802-4812.

Freund, A., Laberge, R.-M., Demaria, M. and Campisi, J. (2012). Lamin B1 loss is a senescence-associated biomarker. *Mol. Biol. Cell* **23**, 2066-2075.

Helt, A.-M. and Galloway, D. A. (2001). Destabilization of the retinoblastoma tumor suppressor by human papillomavirus type 16 E7 is not sufficient to overcome cell cycle arrest in human keratinocytes. *J. Virol.* **75**, 6737-6747.

Ho, K.-K., McGuire, V. A., Koo, C.-Y., Muir, K. W., de Olano, N., Maifoshie, E., Kelly, D. J., Mcgovern, U. B., Monteiro, L. J., Gomes, A. R. et al. (2012). Phosphorylation of FOXO3a on Ser-7 by p38 promotes its nuclear localization in response to doxorubicin. *J. Biol. Chem.* **287**, 1545-1555.

Hydbring, P., Malumbres, M. and Sicinski, P. (2016). Non-canonical functions of cell cycle cyclins and cyclin-dependent kinases. *Nat. Rev. Mol. Cell Biol.* **17**, 280-292.

Jirawatnotai, S., Hu, Y., Michowski, W., Elias, J. E., Becks, L., Bienvenu, F., Zagozdzon, A., Goswami, T., Wang, Y. E., Clark, A. B. et al. (2011). A function for cyclin D1 in DNA repair uncovered by protein interactome analyses in human cancers. *Nature* **474**, 230-234.

Kops, G. J. P. L., Dansen, T. B., Polderman, P. E., Saarloos, I., Wirtz, K. W. A., Coffer, P. J., Huang, T.-T., Bos, J. L., Medema, R. H. and Burgering, B. M. T. (2002). Forkhead transcription factor FOXO3a protects quiescent cells from oxidative stress. *Nature* **419**, 316-321.

Lam, E. W.-F., Brosens, J. J., Gomes, A. R. and Koo, C.-Y. (2013). Forkhead box proteins: tuning forks for transcriptional harmony. *Nat. Rev. Cancer* **13**, 482-495.

Lee, H., Wang, K., Johnson, A., Jones, D. M., Ali, S. M., Elvin, J. A., Yelensky, R., Lipson, D., Miller, V. A., Stephens, P. J. et al. (2016). Comprehensive genomic profiling of extrahepatic cholangiocarcinoma reveals a long tail of therapeutic targets. *J. Clin. Pathol.* **69**, 403-408.

Li, Z., Jiao, X., Wang, C., Shirley, L. A., Elsaleh, H., Dahl, O., Wang, M., Soutoglou, E., Knudsen, E. S. and Pestell, R. G. (2010). Alternative cyclin D1 splice forms differentially regulate the DNA damage response. *Cancer Res.* **70**, 8802-8811.

Luscher-Firzlaff, J. M., Lilischkis, R. and Luscher, B. (2006). Regulation of the transcription factor FOXM1c by Cyclin E/CDK2. *FEBS Lett.* **580**, 1716-1722.

Majumder, P. K., Grisanzio, C., O'connell, F., Barry, M., Brito, J. M., Xu, Q., Guney, I., Berger, R., Herman, P., Bikoff, R. et al. (2008). A prostatic intraepithelial neoplasia-dependent p27Kip1 checkpoint induces senescence and inhibits cell proliferation and cancer progression. *Cancer Cell* **14**, 146-155.

Musgrove, E. A., Caldon, C. E., Barraclough, J., Stone, A. and Sutherland, R. L. (2011). Cyclin D as a therapeutic target in cancer. *Nat. Rev. Cancer* **11**, 558-572.

Narita, M., Nuñez, S., Heard, E., Narita, M., Lin, A. W., Hearn, S. A., Spector, D. L., Hannon, G. J. and Lowe, S. W. (2003). Rb-mediated heterochromatin formation and silencing of E2F target genes during cellular senescence. *Cell* **113**, 703-716.

Nestal de Moraes, G., Bella, L., Zona, S., Burton, M. J. and Lam, E. W.-F. (2016). Insights into a critical role of the FOXO3a-FOXM1 axis in DNA damage response and genotoxic drug resistance. *Curr. Drug Targets* **17**, 164-177.

Otto, T. and Sicinski, P. (2017). Cell cycle proteins as promising targets in cancer therapy. *Nat. Rev. Cancer* **17**, 93-115.

Parameyong, A., Charngkaew, K., Govitrapong, P. and Chetsawang, B. (2013). Melatonin attenuates methamphetamine-induced disturbances in mitochondrial dynamics and degeneration in neuroblastoma SH-SY5Y cells. *J. Pineal Res.* **55**, 313-323.

Rayess, H., Wang, M. B. and Srivatsan, E. S. (2012). Cellular senescence and tumor suppressor gene p16. *Int. J. Cancer* **130**, 1715-1725.

Sakamaki, T., Casimiro, M. C., Ju, X., Quong, A. A., Katiyar, S., Liu, M., Jiao, X., Li, A., Zhang, X., Lu, Y. et al. (2006). Cyclin D1 determines mitochondrial function in vivo. *Mol. Cell. Biol.* **26**, 5449-5469.

Salama, R., Sadaie, M., Hoare, M. and Narita, M. (2014). Cellular senescence and its effector programs. *Genes Dev.* **28**, 99-114.

Salazar-Roa, M. and Malumbres, M. (2017). Fueling the cell division cycle. *Trends Cell Biol.* **27**, 69-81.

Sherr, C. J. and Roberts, J. M. (2004). Living with or without cyclins and cyclin-dependent kinases. *Genes Dev.* **18**, 2699-2711.

Sukov, W. R., Ketterling, R. P., Lager, D. J., Carlson, A. W., Sinnwell, J. P., Chow, G. K., Jenkins, R. B. and Cheville, J. C. (2009). CCND1 rearrangements and cyclin D1 overexpression in renal oncocytomas: frequency, clinicopathologic features, and utility in differentiation from chromophobe renal cell carcinoma. *Hum. Pathol.* **40**, 1296-1303.

Tchakarska, G., Roussel, M., Troussard, X. and Sola, B. (2011). Cyclin D1 inhibits mitochondrial activity in B cells. *Cancer Res.* **71**, 1690-1699.

Trachootham, D., Alexandre, J. and Huang, P. (2009). Targeting cancer cells by ROS-mediated mechanisms: a radical therapeutic approach? *Nat. Rev. Drug Discov.* **8**, 579-591.

Voit, R., Hoffmann, M. and Grummt, I. (1999). Phosphorylation by G1-specific cdk-cyclin complexes activates the nucleolar transcription factor UBF. *EMBO J.*, **18**, 1891-1899.

Vurusaner, B., Poli, G. and Basaga, H. (2012). Tumor suppressor genes and ROS: complex networks of interactions. *Free Radic. Biol. Med.* **52**, 7-18.

Wang, T. C., Cardiff, R. D., Zukerberg, L., Lees, E., Arnold, A. and Schmidt, E. V. (1994). Mammary hyperplasia and carcinoma in MMTV-cyclin D1 transgenic mice. *Nature* **369**, 669-671.

Wang, C., Li, Z., Lu, Y., Du, R., Katiyar, S., Yang, J., Fu, M., Leader, J. E., Quong, A., Novikoff, P. M. et al. (2006). Cyclin D1 repression of nuclear respiratory factor 1 integrates nuclear DNA synthesis and mitochondrial function. *Proc. Natl. Acad. Sci. USA* **103**, 11567-11572.

Ward, P. S. and Thompson, C. B. (2012). Metabolic reprogramming: a cancer hallmark even warburg did not anticipate. *Cancer Cell* **21**, 297-308.

Wu, J., Lee, S.-W., Zhang, X., Han, F., Kwan, S.-Y., Yuan, X., Yang, W.-L., Jeong, Y. S., Rezaeian, A. H., Gao, Y. et al. (2013). Foxo3a transcription factor is a negative regulator of Skp2 and Skp2 SCF complex. *Oncogene* **32**, 78-85.

Yuan, S. S., Lee, S. Y., Chen, G., Song, M., Tomlinson, G. E. and Lee, E. Y. (1999). BRCA2 is required for ionizing radiation-induced assembly of Rad51 complex in vivo. *Cancer Res*. **59**, 3547-3551.

Young, A. P., Schlisio, S., Minamishima, Y. A., Zhang, Q., Li, L., Grisanzio, C., Signoretti, S. and Kaelin, W. G. Jr. (2008). VHL loss actuates a HIF-independent senescence programme mediated by Rb and p400. *Nat. Cell Biol.* **10**, 361-369.

Yu, Q., Geng, Y. and Sicinski, P. (2001). Specific protection against breast cancers by cyclin D1 ablation. *Nature* **411**, 1017-1021.

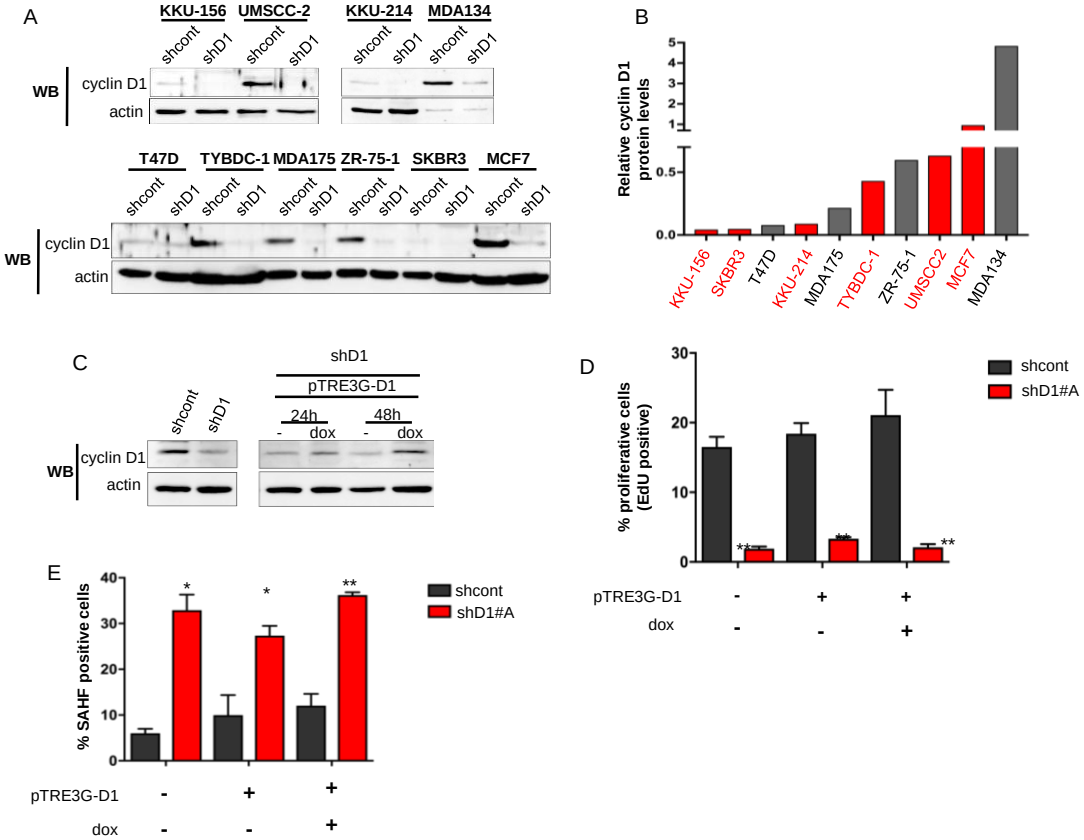

Fig. S1.

A. Western blotting (WB) analysis of cyclin D1-knockdown efficiency in several types of cancer cell lines. Protein lysates were harvested 4 days after transduced with non-targeting shRNA (shcont) or cyclin D1-specific shRNA (shD1#A). Actin was used as a loading control.

B. Relative protein levels of cyclin D1 in the cell lines from (a). Bars in grey are cell lines that did not undergo senescence and red bars are cell lines that underwent senescence upon cyclin D1 depletion.

C. Western blotting (WB) analysis of re-expressing cyclin D1-HA in the senescent cells. The inducible system (Takara Bio Inc., Mountain view, CA, USA), composed of pEF1α-Tet3G and pTRE3G-cyclin D1-HA plasmids was co-transfected into MCF7 cells, followed by cyclin D1 depletion using cyclin D1-specific shRNA (shD1#A). Expression of cyclin D1-HA was achieved by addition of 1 μM doxycycline. Re-expressions of cyclin D1-HA were examined at 24 and 48 hours after the induction. Actin was used as a loading control.

D. Re-expression of cyclin D1-HA did not increase cell proliferation in cyclin D1 depletion-induced senescent cells. Percentages of EdU-positive cells were analyzed at 48 hours after the induction. Bars represent averages of 3 experiments± s.d. (**$p \leq 0.01$)

E. Re-expression of cyclin D1-HA in the senescent cells did not reduced number of SAHF-positive cell. Analyses of SAHF-positive cell numbers were performed at the same time point as in (d). Doxycycline treatment; dox. Bars represent averages of 3 experiments ± s.d. (*$p \leq 0.05$ and **$p \leq 0.01$)

Statistical significance was determined by Student's t-test

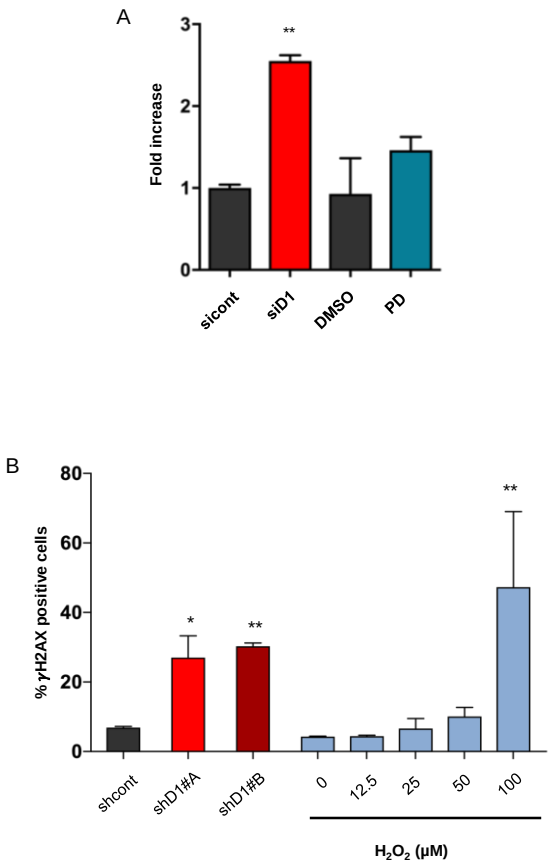

Fig. S2.

A. Apoptosis detection of cyclin D1-specific siRNA (siD1) and CDK4/6 inhibitor treatment (PD), compared to control cells (sicont) and vehicle control (DMSO). Bars represent averages from 3 independent experiments ± s.d. Statistical significance was determined by Student's t-test (***p*≤*0.01*).

B. Cyclin D1-depleted cells (shD1#A, shD1#B) showed significant elevation of γH2AX foci-positive cells, compared to control cells (shcont). Percentages of γH2AX foci-positive MCF7 cells treated with increasing concentrations of H_2O_2 are shown as a reference (grey bars). At least 5,000 γH2AX-positive cells were analyzed. Bars represent averages from 3 independent experiments ± s.d. Statistical significance was determined by Student's t-test (**p*≤*0.05 and* ***p*≤*0.01*).

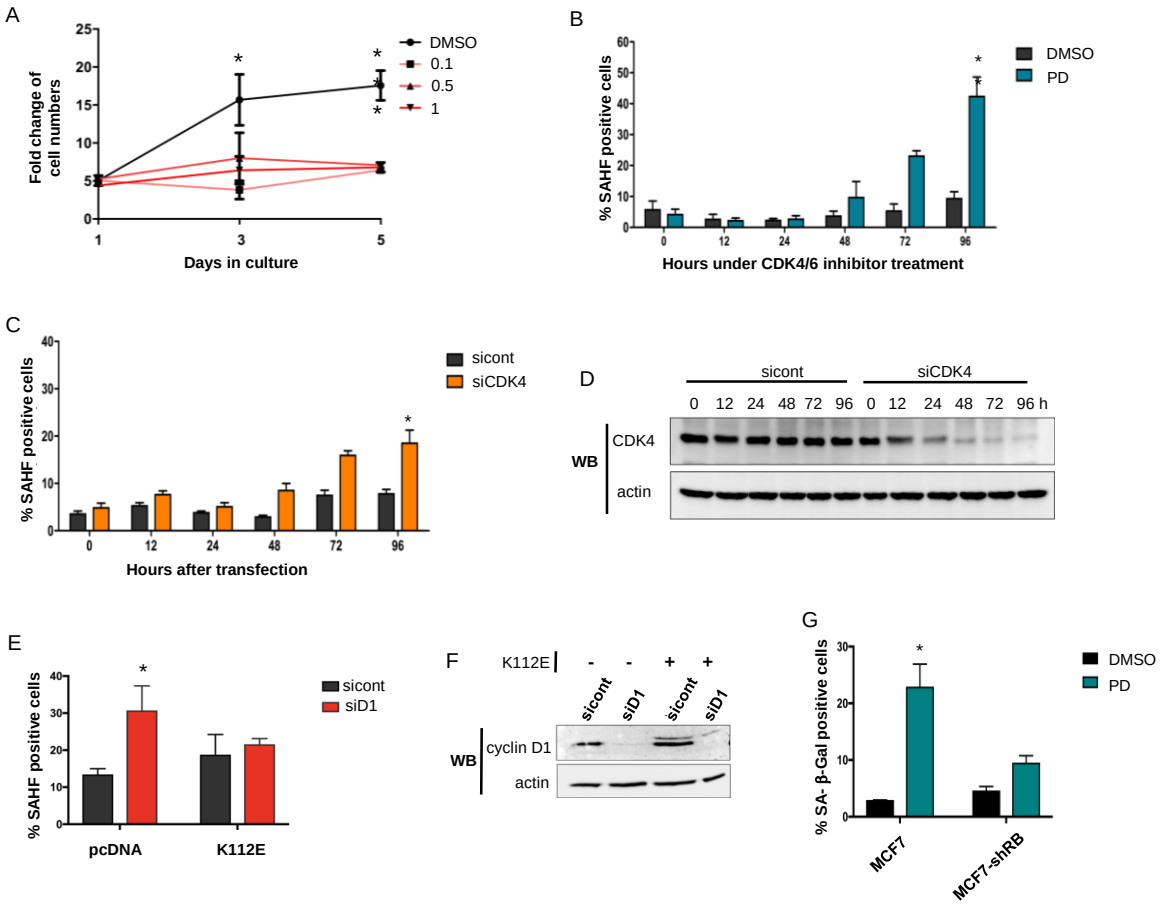

Fig. S3.

A. Growth curves of MCF7 cells treated with CDK4/6 inhibitor (PD) at indicated concentration (0, 0.1, 0.5, and 1 μM).

B. Percentages of SAHF-positive MCF7 cells were analyzed at 0, 12, 24, 48, 72, and 96 hours after the cells were treated with 0.5 μM PD 0332991 (PD). DMSO was use as a vehicle control. Bars represent averages from 3 independent experiments ± s.d. *(**p≤0.01*).

C. Percentages of SAHF-positive MCF7 cells were analyzed at 0, 12, 24, 48, 72, and 96 hours after the cells were transfected with CDK4-specific siRNA (siCDK4), or non-target control siRNA (sicont). Bars represent averages from 3 independent experiments ± s.d. *(*p≤0.05*).

D. WB analysis of CDK4 depletion by the CDK4-specific siRNA at indicated time points as in (c). Actin was used as a loading control.

E. Cells were co-transfected control pladmid pcDNA or kinase dead cyclin D1 (K112E), with GFP expressing plasmid peGFP, followed by cyclin D1 depletion using cyclin D1-specific siRNA targeting 5'UTR of cyclin D1 mRNA. Percentages of SAHF-positive MCF7 cells were analyzed in GFP-positive cells after 72 hours of cyclin D1 depletion (**p≤0.05*).

F. WB analysis of MCF7 cells expressing kinase-dead cyclin D1 (K112E). Lysates were collected after 72 hours of siRNA transfection.

G. Percentages of SA-β-Gal-positive cells after 5 days of PD0332991 (PD) or vehicle (DMSO) treatment . Bars represent averages from 3 independent experiments ± s.d. (**p≤0.05*).

Statistical significance was determined by Student's t-test

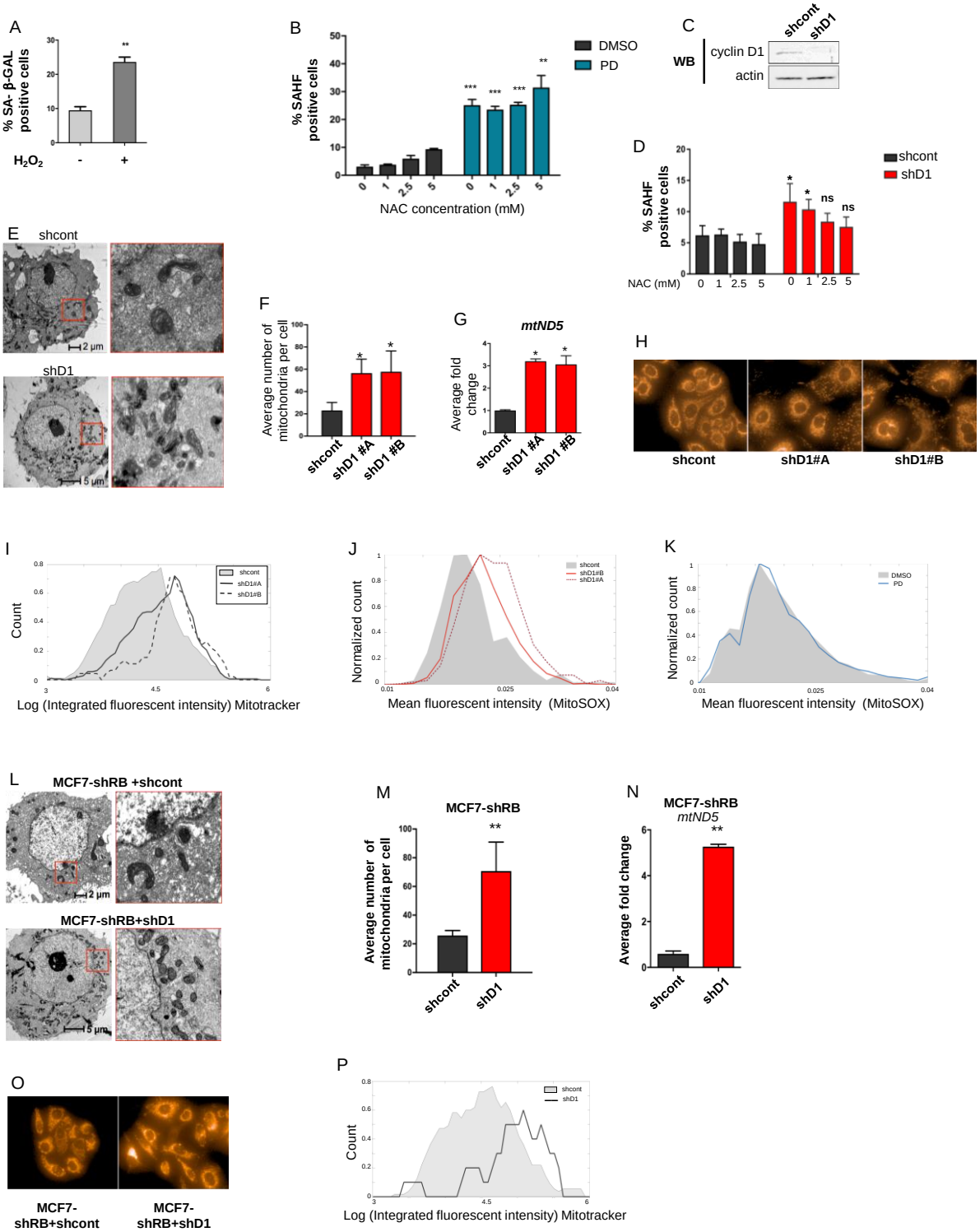
A
% SA- β-GAL positive cells
H2O2
B
% SAHF positive cells
DMSO
PD
NAC concentration (mM)
C
shcont
shD1
WB
cyclin D1
actin
D
% SAHF positive cells
shcont
shD1
NAC (mM)
E
shcont
shD1
2 µm
5 µm
F
Average number of mitochondria per cell
shcont
shD1 #A
shD1 #B
G
mtND5
Average fold change
H
shcont
shD1#A
shD1#B
I
Count
Log (Integrated fluorescent intensity) Mitotracker
J
Normalized count
Mean fluorescent intensity (MitoSOX)
K
Normalized count
DMSO
PD
Mean fluorescent intensity (MitoSOX)
L
MCF7-shRB +shcont
MCF7-shRB+shD1
M
MCF7-shRB
Average number of mitochondria per cell
N
MCF7-shRB
mtND5
Average fold change
O
MCF7-shRB+shcont
MCF7-shRB+shD1
P
Count
Log (Integrated fluorescent intensity) Mitotracker

Fig. S4.

A. MCF7 cells were treated with 1000 μM of H_2O_2 for 72 hours. Bars represent average percentages ± s.d. of SA-β-Gal-positive cells from 3 experiments *(**p≤0.01*)

B. PD0332991-induced senescence could not be prevented by N-acetyl cysteine (NAC). Percentages of SAHF-positive MCF7 cells were analyzed after 96 hours of 0.5 μM PD0332991 (PD) treatment. Indicated concentrations of NAC were added to the culture medium at the same time as PD treatment. DMSO was used as vehicle control. Bar represent average ± s.d *(**p≤0.01, ***p≤0.001*)

C. WB analysis of cyclin D1 in Capan-1 cells after transduced with non-targeting shRNA (shcont) or cyclin D1 shRNA (shD1) for 4 days.

D. Percentages of SAHF-positive Capan-1 cells were analyzed after transfected with non-targeting shRNA (shcont) or cyclin D1 shRNA (shD1) for 4 days . Indicated concentrations of NAC were added to the culture medium at the same time as cyclin D1 depletion. Bar represent average ± s.d *(*p≤0.05, ns; statistically not significant)*

E. MCF7 cells were transduced with non-targeting shRNA (shcont) or cyclin D1 shRNA (shD1) for 4 days before analyzed by transmission electron microscope (TEM). Red boxes are enhanced to the right figures.

F. Average numbers of mitochondria per cell analyzed by TEM from (c) (shcont; n = 4 cells) (shD1 #A, and #B; n = 5 cells). Bars represent averages of 3 experiments ± s.d. (**p≤0.05*)

G. Mitochondrial DNA contents of *mtND5* gene in cyclin D1-depleted, and control cells. Bars represent averages of 3 experiments ± s.d. (**p≤0.05*)

H. Mitotracker staining of MCF7 cells expressing non-targeting control shRNA (shcont), or cyclin D1-specific shRNAs (shD1#A, and shD1#B).

I. Histograms show Log integrated fluorescent intensity of Mitotracker stained mitochondria from MCF7 cells expressing either non-targeting shRNA (shcont), or cyclin D1-specific shRNAs (shD1#A, and shD1#B), from (f).

J. Histograms show mean fluorescent intensities of MitoSox Red stained mitochondria in MCF7 cells expressing either non-targeting shRNA (shcont), or cyclin D1-specific shRNAs (shD1#A, and shD1#B).

K. Histograms show mean fluorescent intensities of MitoSox Red stained mitochondria in MCF7 cells treated either with vehicle (DMSO), or 0.5μM PD0332991 (PD)

L. TEM analyses of pRB-deficient MCF7 cells (upper panel) and pRB-deficient MCF7 cells expressing cyclin D1-specific shRNA (shD1# C) (lower panel). Red boxes are enhanced to the right figures.

M. Average numbers of mitochondria per cell from (L). Bars represent averages ± s.d. (shcont, n = 5 cells; shD1, n = 5 cells) (**p≤0.01*)

N. Mitochondrial DNA content of *mtND5* gene in MCF7-shRB cells. Bars represent averages ± s.d. from 3 experiments (**p≤0.01*)

O. Mitotracker staining of MCF7-shRB cells expressing non-targeting shRNA (shcont), or a cyclin D1-specific shRNA (shD1#C).

P. Histograms show log integrated fluorescence intensity of Mitotracker stained mitochondria from MCF7-shRB cells expressing either control shcont (shcont), or cyclin D1-specific shRNA (shD1), from (m).

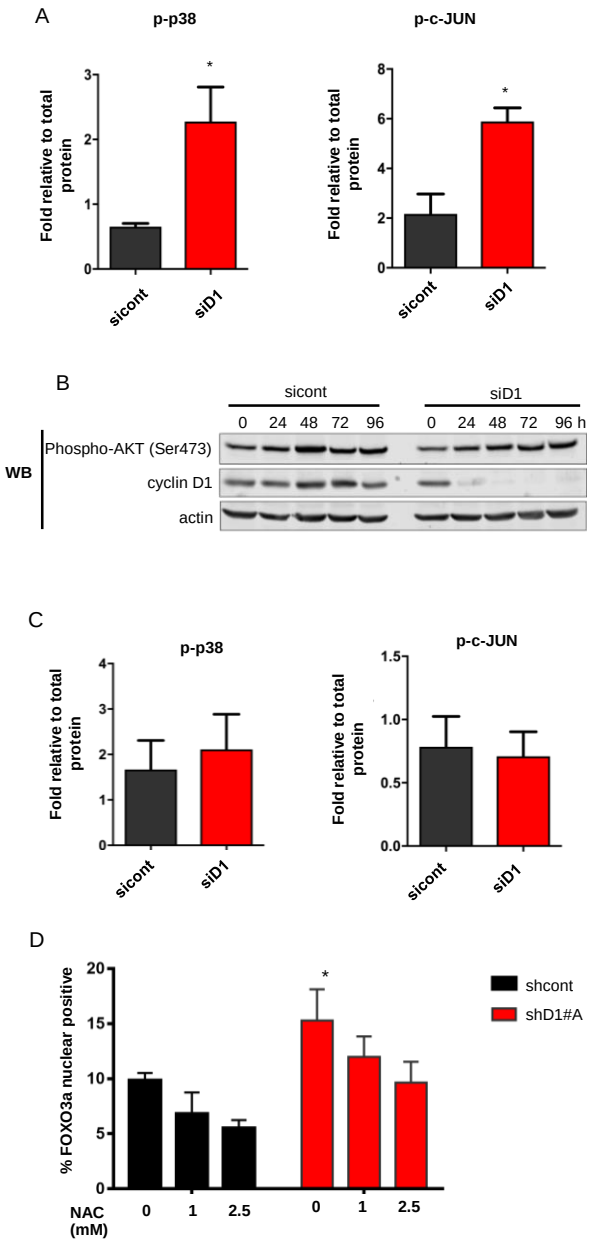

Fig. S5.

A. Cells were transfected with non-targeted siRNA (sicont) or cyclin D1 siRNA (siD1) transfection. Bars represent quantified signals of phospho-p38, and phospho-c-JUN normalized by total proteins at the 96-hour time point. (**p≤0.05*)
B. WB analysis of phospho-AKT Ser473, and cyclin D1 after transfected with with non-targeted siRNA (sicont) or cyclin D1 siRNA (siD1) at indicated time points. Actin was used as a loading control.
C. WB analysis was performed similarly as in **(A)**, except that freshly prepared NAC was added to the cells every other day from the 0 hour until the cells were harvested. Bars represent quantified signals of phospho-p38, and phospho-c-JUN normalized by total proteins at the 96-hour time point.
D. MCF7 cells were transduced with non-targeting shRNA (shcont) or cyclin D1 shRNA (shD1) for 4 days under treatment of NAC at indicated concentration. At least 5,000 FOXO3a nuclear-positive cells were analyzed. Bars represent percentage of cell that have nuclear FOXO3a localization. *(*p≤0.05*).

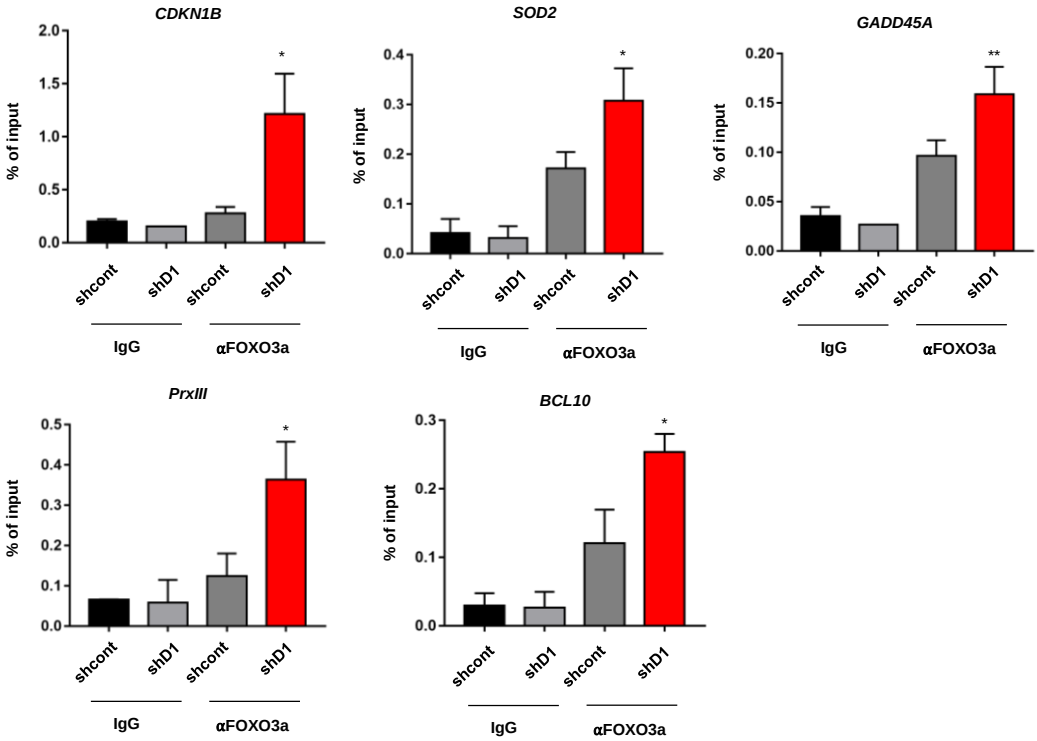

Fig. S6.

FOXO3a chromatin immunoprecipitation (ChIP) in cells expressing non-targeting shRNA (shcont) or cyclin D1 shRNA (shD1). ChIP products were analyzed by semi-quantitative PCRs. IgG was used as a negative control for chromatin immunoprecipitation. Bars represent percent of input ± s.d. *(*p≤0.05, **p≤0.01*).

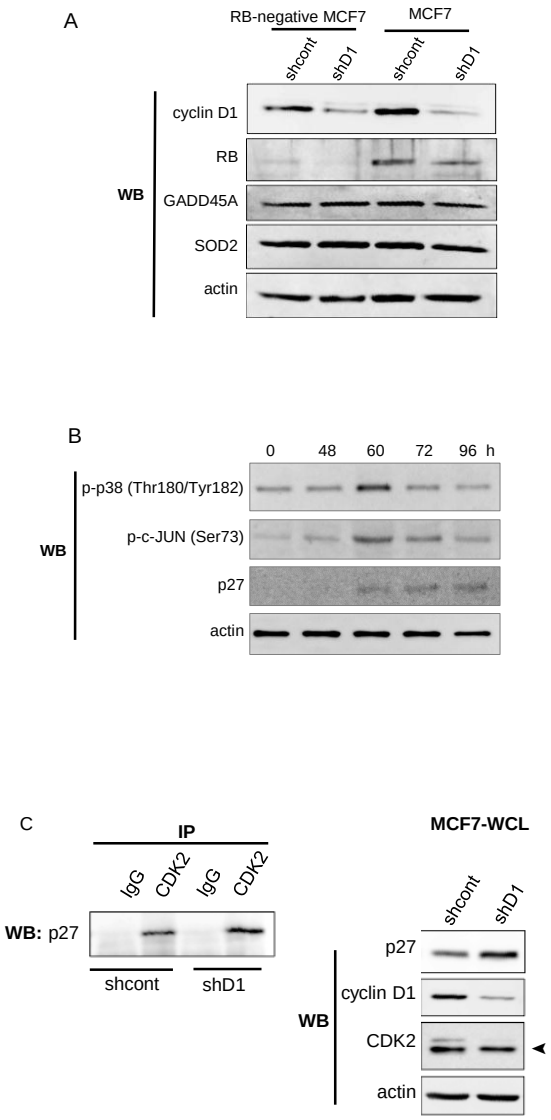

Fig. S7.

A. MCF7 cells and MCF7-expressing shRB were transduced with non-targeting shRNA (shcont) or cyclin D1 shRNA (shD1#C). Four days after transduction the cell lysates were collected and indicated proteins were analyzed by WB analyses. Actin was used as a loading control.

B. The upregulation of p27 coincided with p38 and c-JUN phosphorylations. WB analysis of p27, and p38/c-JUN specific phosphorylations. Protein lysates were prepared at 0, 48, 60, 72, and 96 hours after cyclin D1 siRNA (siD1) transfection.

C. (Left) WB analysis of p27 from immunoprecipitation by using IgG or CDK2 antibody in MCF7 cells expressing non-targeting shRNA (shcont) or cyclin D1 shRNA (shD1). (Right) WB analyses of whole cell lysate (WCL) from MCF7 cell with non-targeting shRNA (shcont), or cyclin D1 shRNA (shD1). Arrow indicated the CDK2 band.